



**HAL**  
open science

## Chemical Synthesis of TFF3 Reveals Novel Mechanistic Insights and a Gut-Stable Metabolite

Nayara Braga Emidio, Rajeshwari Meli, Hue Tran, Hayeon Baik, Séverine Morisset-Lopez, Alysha Elliott, Mark Blaskovich, Sabrina Spiller, Annette Beck-Sickinger, Christina Schroeder, et al.

► **To cite this version:**

Nayara Braga Emidio, Rajeshwari Meli, Hue Tran, Hayeon Baik, Séverine Morisset-Lopez, et al.. Chemical Synthesis of TFF3 Reveals Novel Mechanistic Insights and a Gut-Stable Metabolite. *Journal of Medicinal Chemistry*, 2021, 64 (13), pp.9484-9495. 10.1021/acs.jmedchem.1c00767 . hal-03335490

**HAL Id: hal-03335490**

**<https://hal.science/hal-03335490v1>**

Submitted on 21 Nov 2021

**HAL** is a multi-disciplinary open access archive for the deposit and dissemination of scientific research documents, whether they are published or not. The documents may come from teaching and research institutions in France or abroad, or from public or private research centers.

L'archive ouverte pluridisciplinaire **HAL**, est destinée au dépôt et à la diffusion de documents scientifiques de niveau recherche, publiés ou non, émanant des établissements d'enseignement et de recherche français ou étrangers, des laboratoires publics ou privés.

# 1 Chemical Synthesis of TFF3 Reveals Novel Mechanistic Insights and 2 a Gut-Stable Metabolite

3 Nayara Braga Emidio, Rajeshwari Meli, Hue N. T. Tran, Hayeon Baik, Séverine Morisset-Lopez,  
4 Alysha G. Elliott, Mark A. T. Blaskovich, Sabrina Spiller, Annette G. Beck-Sickinger,  
5 Christina I. Schroeder, and Markus Muttenthaler\*



Cite This: <https://doi.org/10.1021/acs.jmedchem.1c00767>



Read Online

ACCESS |



Metrics & More

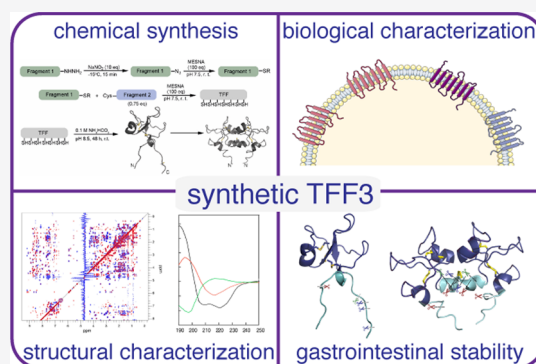


Article Recommendations



Supporting Information

6 **ABSTRACT:** TFF3 regulates essential gastro- and neuroprotective  
7 functions, but its molecular mode of action remains poorly understood.  
8 Synthetic intractability and lack of reliable bioassays and validated receptors  
9 are bottlenecks for mechanistic and structure–activity relationship studies.  
10 Here, we report the chemical synthesis of TFF3 and its homodimer *via* native  
11 chemical ligation followed by oxidative folding. Correct folding was  
12 confirmed by NMR and circular dichroism, and TFF3 and its homodimer  
13 were not cytotoxic or hemolytic. TFF3, its homodimer, and the trefoil  
14 domain (TFF3<sub>10–50</sub>) were susceptible to gastrointestinal degradation,  
15 revealing a gut-stable metabolite (TFF3<sub>7–54</sub>;  $t_{1/2}$  > 24 h) that retained its  
16 trefoil structure and antiapoptotic bioactivity. We tried to validate the  
17 putative TFF3 receptors CXCR4 and LINGO2, but neither TFF3 nor its  
18 homodimer displayed any activity up to 10  $\mu$ M. The discovery of a gut-stable  
19 bioactive metabolite and reliable synthetic accessibility to TFF3 and its analogues are cornerstones for future molecular probe  
20 development and structure–activity relationship studies.



## 21 ■ INTRODUCTION

22 The trefoil factor family (TFF) comprises three disulfide-rich  
23 peptides (TFF1, TFF2, TFF3) that are abundantly secreted in  
24 the gastrointestinal tract where they regulate gut homeostasis  
25 by promoting gut protection and repair.<sup>1–5</sup> They are also  
26 expressed in mucosal tissues outside the gut, including in the  
27 respiratory tract, urinary tract, uterus, eyes, and salivary glands,  
28 where they have similar mucosal repair and protective  
29 functions. TFF peptides have also been observed in human  
30 breast milk and the brain,<sup>1,6,7</sup> and have been implicated in  
31 cancer development.<sup>1,8,9</sup>

32 TFF3 is highly expressed in the gastrointestinal mucosa,  
33 particularly in the small intestine and colon, where it protects,  
34 maintains, and repairs the gastrointestinal tract.<sup>4,10–17</sup> In the  
35 central nervous system (CNS), TFF3 is secreted by neurons  
36 and regulates physiological effects such as neuroinflammation<sup>18</sup>  
37 and behavioral processes including learning and memory<sup>19</sup> and  
38 depression.<sup>20,21</sup> The anti-inflammatory effects of TFF3 on  
39 microglia cells (reduced expression and secretion of pro-  
40 inflammatory cytokines) and its capacity to mitigate ischemic  
41 cerebral injuries by reducing cell death *via* suppression of  
42 caspase-3 activity further support TFF3's neuroprotective role  
43 in the CNS.<sup>18,22</sup>

44 TFF3 derives from a 94-residue long precursor protein that  
45 comprises a 35-residue-long signal peptide followed by the 59-  
46 residue-long TFF3 sequence.<sup>23</sup> The mature secreted and

folded TFF3 peptide (TFF3<sub>1–59</sub>) contains a highly conserved  
47 trefoil domain (TFF3<sub>10–50</sub>) that also defines the other members  
48 of the TFF.<sup>3,24</sup> The trefoil domain contains six conserved  
49 cysteine residues (CX<sub>9–10</sub>CX<sub>9</sub>CX<sub>4</sub>CCX<sub>10</sub>C motif) forming  
50 three intrachain disulfide bonds in the configuration Cys<sup>I–V</sup>,  
51 Cys<sup>II–IV</sup>, and Cys<sup>III–VI</sup>.<sup>3,24</sup> This disulfide bond arrangement  
52 creates a compact three-loop structure resembling a trefoil  
53 shape, which is considered to be metabolically stable based on  
54 TFF3's functional role in the gastrointestinal tract.<sup>3,24,25</sup> Its  
55 gastrointestinal stability has, however, not been systematically  
56 investigated, and some reports indicate that TFF3 might not be  
57 that stable.<sup>26–28</sup>

58 TFF3 also has an additional C-terminal cysteine residue  
59 (Cys<sup>VII</sup>) located outside the trefoil domain, which enables the  
60 formation of covalent homo- or heterodimers (e.g., with the  
61 mucus-associated Fc fragment of IgG Fc binding protein,  
62 FCGBP).<sup>29,30</sup> TFF3-FCGBP's function remains unknown, but  
63 it is hypothesized to act as a TFF3 reservoir.<sup>29</sup> Although the  
64 TFF3 homodimer is only present in relatively small  
65

Received: April 28, 2021

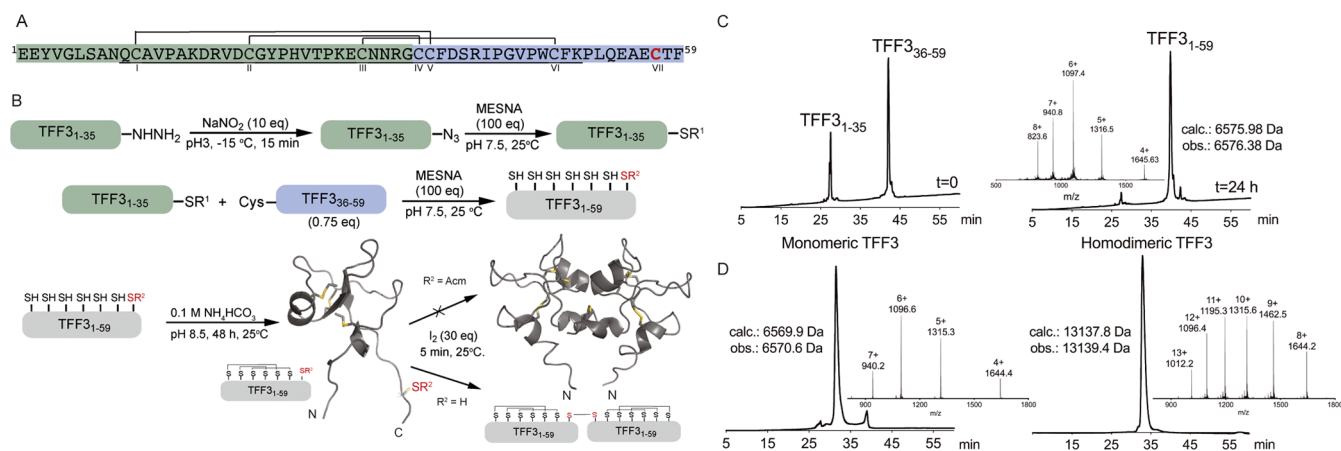


**Figure 1.** Synthesis of TFF3 and its homodimer. (A) TFF3 sequence and disulfide bond connectivity. Sequence highlighted in green and blue represents the N- and C-terminal fragments used for native chemical ligation, respectively, with Cys<sup>57</sup> (red) used for dimerization. The trefoil domain is underlined. (B) Synthetic strategy used to produce TFF3 and its homodimer. Highlighted in gray is full-length TFF3. (C) Ligation reaction at time 0 h (left) and 24 h (right). (D) Analytical RP-HPLC chromatogram and MS of folded TFF3 monomer (left) and homodimer (right). TFF3 monomer displays a two-peak RP-HPLC profile due to its conformational complexity (see also Figure S3). TFF3 PDB: 1E9T; TFF3 homodimer PDB: 1PE3.

66 quantities,<sup>29</sup> it is more potent than its monomeric counterpart  
67 in promoting cell motility.<sup>31,32</sup> Additionally, only the  
68 homodimer but not the monomer displays protective effects  
69 when luminally administered in an experimental model of  
70 colitis.<sup>32</sup>

71 TFF3 can induce several biological effects (i.e., antiapopto-  
72 tic,<sup>33,34</sup> cell migration,<sup>35–37</sup> and anti-inflammatory effects<sup>38</sup>),  
73 but its mode of action and target receptors have not been fully  
74 elucidated nor validated.<sup>30</sup> TFF3 was recently described as a  
75 natural ligand of the leucine-rich repeat receptor and nogo-  
76 interacting protein 2 (LINGO2),<sup>38</sup> with TFF3-LINGO2  
77 interaction mediating intestinal wound healing and immunity  
78 through enhanced epidermal growth factor receptor (EGFR)  
79 signaling.<sup>38</sup> Another putative receptor is the chemokine  
80 receptor type 4 (CXCR4), through which TFF3 might  
81 mediate cell migration *via* an ERK1/2-independent signaling  
82 pathway.<sup>39</sup>

83 TFF3 is considered a promising therapeutic lead, especially  
84 for disorders requiring epithelial protection, repair, or  
85 restitution, such as inflammatory bowel diseases (IBD) and  
86 nonsteroidal anti-inflammatory drug-induced gastritis.<sup>30</sup> Its  
87 therapeutic potential is supported by promising preclinical  
88 <sup>11,40–42</sup> and clinical studies.<sup>30,43,44</sup> TFF3 is currently  
89 obtained either through recombinant production in *Escherichia*  
90 *coli*, *Saccharomyces cerevisiae*, or human embryonic kidney 293  
91 (HEK-293) cells,<sup>45–47</sup> or through purification from milk<sup>48</sup> or  
92 meconium.<sup>49</sup> These approaches are however not ideal for drug  
93 target discovery, where advanced probe development is  
94 required, nor for drug development efforts where the  
95 incorporation of unnatural amino acids, reporter tags, or  
96 conjugation handles at specific positions is often required.  
97 Chemical synthesis would allow for such regiospecific control  
98 and incorporation of unnatural amino acids, thereby  
99 considerably facilitating mechanistic studies and therapeutic  
100 development. We thus set out to establish a synthetic strategy  
101 to produce TFF3 and its homodimer reliably and in sufficient  
102 quantities to deliver new insights into their pharmacology,  
103 toxicity, and metabolic stability.

## RESULTS

### Chemical Synthesis of TFF3, TFF3(C<sup>57</sup>Acm), and TFF3 Homodimer.

Single-chain assembly of full-length TFF3<sub>1-59</sub> was not successful due to difficult sequence sections. We therefore switched to a two-fragment native chemical ligation (NCL) approach using the Fmoc-SPPS (9-fluorenylmethoxycarbonyl-solid-phase peptide synthesis)-compatible hydrazide strategy (Figure 1).<sup>50</sup> We split the TFF3 sequence into an N-terminal TFF3<sub>1-35</sub> fragment with a glycine at the ligation site (faster ligation due to less steric hindrance) and a C-terminal TFF3<sub>36-59</sub> fragment with an N-terminal cysteine residue at the ligation site (Figure 1A). We synthesized TFF3<sub>1-35</sub> with a C-terminal hydrazide function (~15% yield after purification) on a freshly prepared 2-Cl-(Trt)-NHNH<sub>2</sub> resin and TFF3<sub>36-59</sub> with a C-terminal acid (~20% yield after purification) using a Phe-Wang PS resin. We activated TFF3<sub>1-35</sub>-NHNH<sub>2</sub> with NaNO<sub>2</sub> to form the C-terminal acyl azide followed by conversion of the azide into a thioester through addition of sodium 2-mercaptoethanesulfonate (MESNA) (Figure 1B).<sup>50</sup> We then ligated the two fragments (TFF3<sub>1-35</sub> and TFF3<sub>36-59</sub>) to produce the linear and fully reduced TFF3<sub>1-59</sub> and purified it on a C<sub>18</sub>-RP-HPLC column (~57% ligation yield) (Figure 1B,C).

After oxidative folding (0.1 M ammonium bicarbonate, pH 8.5, 48 h; Figure S1), we purified TFF3 on a C<sub>5</sub>-RP-HPLC column (Figure 1D, left). The TFF3 homodimer was produced *via* the formation of an intermolecular disulfide bond of unprotected Cys<sup>VII</sup> (residue 57) through treatment with iodine (2 min) followed by C<sub>5</sub>-RP-HPLC purification (Figure 1D, right; 60% yield). Since dimerization of TFF3 with the unprotected Cys<sup>VII</sup> residue was observed in aqueous solvents at pH > 7, we also synthesized a TFF3 analogue with Cys<sup>VII</sup> protected with an acetamidomethyl (Acm) group (TFF3-(C<sup>57</sup>Acm)) to prevent dimerization and to ensure clear functional distinction between monomeric and homodimeric TFF3 in further studies (Figure S1).

Folded TFF3, whether with Cys<sup>VII</sup> protected or not, displayed a two-peak profile on analytical HPLC, with each peak having the correct mass (Figures 1D and S2). When these peaks were independently collected and reinjected, the same

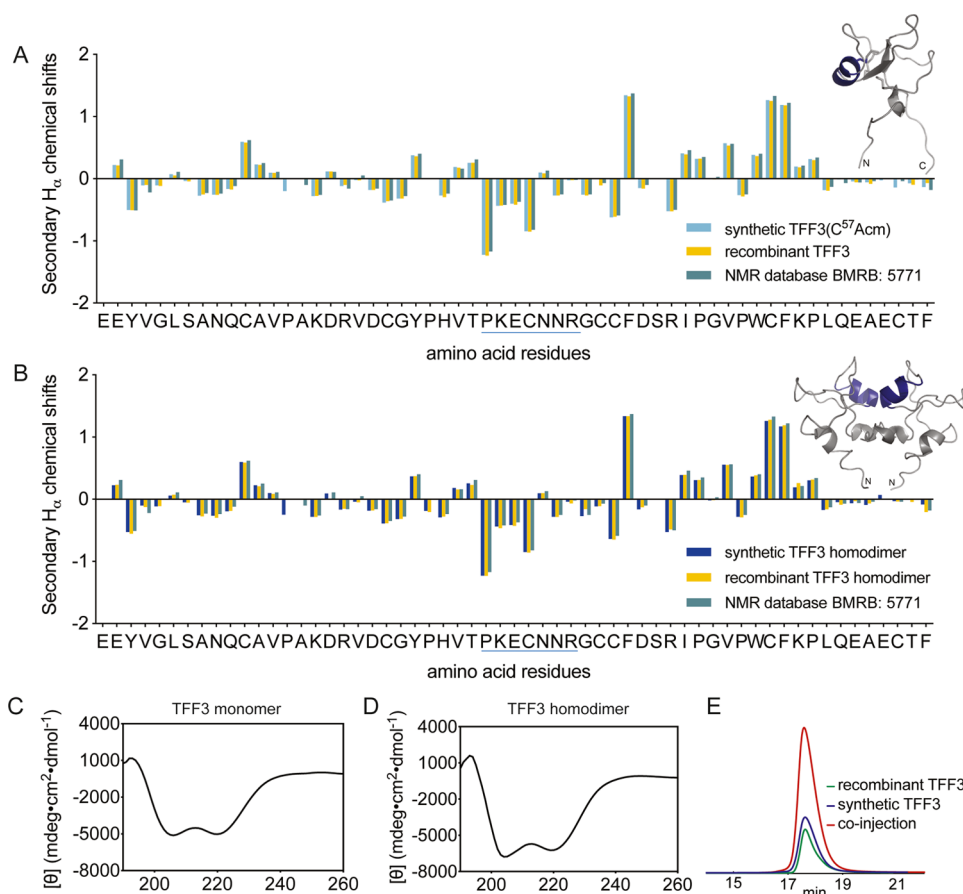


**Figure 2.** Comparison of secondary  $H_{\alpha}$  chemical shifts of (A) TFF3( $C^{57}Acm$ ) and (B) TFF3 homodimer produced by chemical synthesis with recombinant homologues and reported values from the Biological Magnetic Resonance Data Bank (BMRB: 5771). Secondary  $H_{\alpha}$  chemical shifts were determined by subtracting the shifts observed in random coil peptides from the shifts determined from the two-dimensional (2D) NMR analysis.<sup>57</sup> An  $\alpha$ -helical region is highlighted in blue in the sequence and NMR structure. CD spectra of synthetic (C) TFF3( $C^{57}Acm$ ) and (D) TFF3 homodimer. (E) Co-elution of synthetic and recombinant TFF3 homodimer (1:2 ratio) on a  $C_3$ -RP-HPLC (1% gradient).

144 two-peak profile was observed (Figure S3), confirming that  
 145 both peaks belong to TFF3. This is consistent with the  
 146 conformational complexity of TFF3<sup>45</sup> and an effect commonly  
 147 observed with similarly complex peptides and proteins,  
 148 including TFF1.<sup>51–55</sup>

149 **Synthetic TFF3 and TFF3 Homodimer Have the**  
 150 **Correct Fold.** We characterized folded TFF3 and TFF3  
 151 homodimer by nuclear magnetic resonance (NMR) and  
 152 circular dichroism (CD) experiments and compared them  
 153 with the structures of recombinant TFF3 and TFF3  
 154 homodimer.<sup>24,56</sup> The  $H_{\alpha}$  chemical shifts of TFF3( $C^{57}Acm$ )  
 155 and TFF3 homodimer were assigned using total correlated  
 156 spectroscopy (TOCSY) and nuclear Overhauser effect spec-  
 157 troscopy (NOESY). Secondary chemical shifts were deter-  
 158 mined by subtracting random coil shifts from the  $H_{\alpha}$  chemical  
 159 shifts.<sup>57</sup> Comparison of the secondary chemical shift of  
 160 synthetic and recombinantly expressed TFF3 (Figure 2A), as  
 161 well as those of the corresponding homodimers (Figure 2B),  
 162 confirmed the correct fold.<sup>24,56</sup> CD analysis of synthetic TFF3  
 163 indicated the presence of an  $\alpha$ -helical structure characterized  
 164 by negative bands at 222 and 208 nm and a positive band at  
 165 193 nm (Figure 2C,D). This aligned well with the structural  
 166 information obtained from recombinant TFF3 provided by Dr.  
 167 Lars Thim (Novo Nordisk A/S)<sup>45</sup> that has a well-defined  $\alpha$ -  
 168 helix in loop 2. A co-elution study of synthetic and

recombinant TFF3 homodimer further confirmed the NMR 169  
 and CD results (Figure 2E). 170

**TFF3 and TFF3 Homodimer Reduce Apoptosis of** 171  
**Neuroblastoma Cells.** The antiapoptotic activity of TFF3 172  
 was reported in cerebral ischemia.<sup>22</sup> We therefore evaluated 173  
 the capacity of TFF3 and its homodimer to reduce etoposide- 174  
 induced cell death, by inhibiting caspase-3/7, in a neuro- 175  
 blastoma cell line (SH-SY5Y). TFF3 and its homodimer (10 176  
 $\mu M$ ) induced a statistically significant ( $p < 0.05$ ) reduction in 177  
 cell death (Figure 3A). 178

**TFF3 and TFF3 Homodimer Are Not Cytotoxic or** 179  
**Hemolytic.** Considering the therapeutic potential of TFF3, it 180  
 was important to determine any cytotoxic and hemolytic 181  
 effects early on to avoid problems in later stages of drug 182  
 development. We therefore assessed cytotoxicity on HEK-293 183  
 cells and hemolytic effects in human erythrocytes. We treated 184  
 the cells with TFF3( $C^{57}Acm$ ) and TFF3 homodimer and used 185  
 resazurin, a blue dye that produces strong fluorescence when 186  
 reduced by living cells, as the readout of the number of viable 187  
 cells.<sup>60</sup> In the hemolytic assay, we evaluated hemoglobin 188  
 release, an indicator of erythrocyte lysis, upon exposure to the 189  
 peptides. Neither TFF3( $C^{57}Acm$ ) nor TFF3 homodimer 190  
 displayed any cytotoxic or hemolytic effects at the concentra- 191  
 tions of up to  $\sim 25 \mu M$  (Figure 3B,C). 192

**TFF3 and TFF3 Homodimer Do Not Activate CXCR4** 193  
**in COS-7 Cells Overexpressing the Receptor.** CXCR4 is a 194



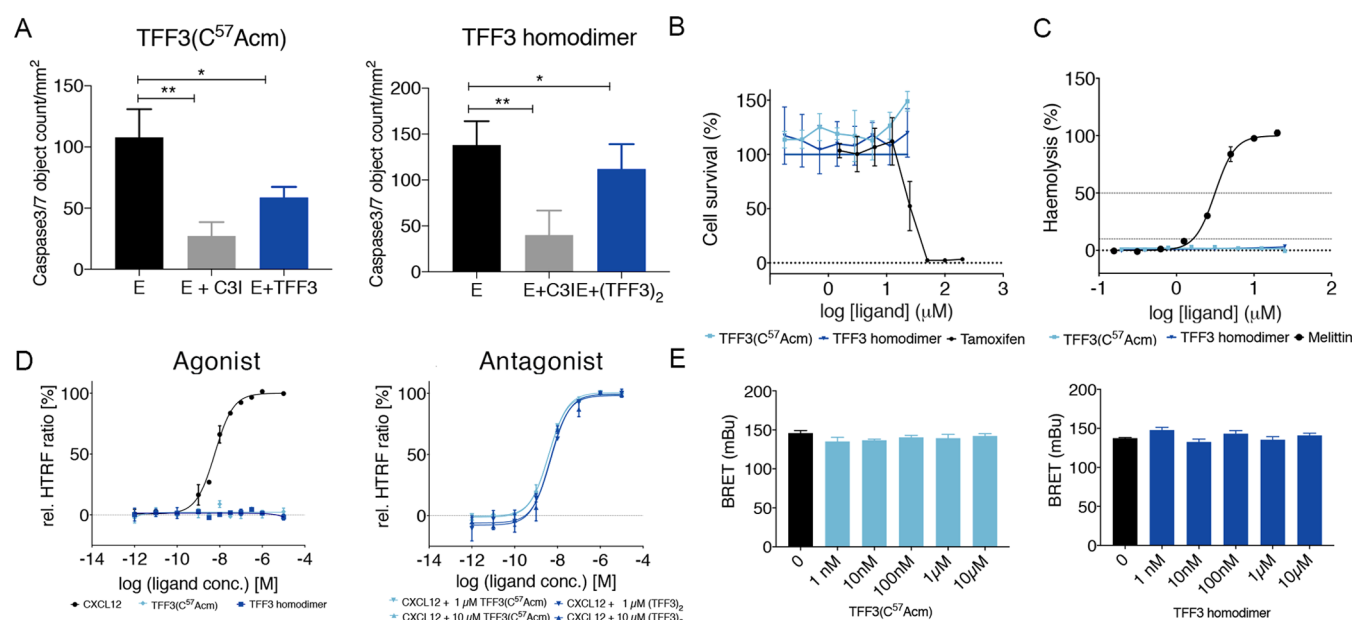


**Figure 3.** Biological characterization of TFF3(C<sup>57</sup>Acm) and TFF3 homodimer. (A) Cell death was induced with etoposide (10  $\mu$ M), and cells were treated with 10  $\mu$ M of TFF3. Etoposide and TFF3 were added at the same time. Caspase-3/7 activity was measured after 6 h. The results are expressed (mean  $\pm$  standard error of the mean (SEM)) of  $n \geq 3$  independent experiments as the number of green fluorescent caspase-3/7 active objects generated by caspase-3/7 reagent added in media. Z-DEVD-FMK (50  $\mu$ M; caspase-3 inhibitor) was used as the positive control. E: etoposide, E + C3I: etoposide + caspase-3 inhibitor. One-way analysis of variance (ANOVA) followed by Dunnett correction was performed to assess differences between treated cells and etoposide only. \* $p < 0.05$ , \*\* $p < 0.01$ . (B) TFF3 effect on the viability of HEK-293 cells after 20 h. Tamoxifen was used as a positive control for cell growth inhibition. Data are representative of two independent experiments shown as mean  $\pm$  SEM. (C) Hemolytic activity of TFF3 after 1 h on erythrocytes. Melittin was used as a positive hemolytic control. Data are representative of two independent experiments shown as mean  $\pm$  SEM. (D) Effect on CXCR4. Agonistic or antagonistic effects were assessed by the IP1 accumulation assay obtained through homogeneous time-resolved fluorescence (HTRF). CXCL12 was added for antagonistic studies after a 5 min preincubation of TFF3(C<sup>57</sup>Acm) or homodimer. For agonistic evaluation, all compounds were used individually for stimulation in the given concentration range.<sup>58</sup> Neither TFF3(C<sup>57</sup>Acm) nor TFF3 homodimer were able to activate or inhibit the signal transduction of CXCR4 at concentrations up to 10  $\mu$ M, indicating that these peptides are neither agonists nor antagonists at this receptor. The results are expressed as mean  $\pm$  SEM of  $n \geq 2$  independent experiments. (E) Effect on LINGO2. HEK-293 coexpressing LINGO2-YFP and LINGO2-Rluc were stimulated with increasing amounts of TFF3(C<sup>57</sup>Acm) and TFF3 homodimer (1 nM–10  $\mu$ M), but no significant increase in the bioluminescence resonance energy transfer (BRET) signal was observed. No ligand able to alter LINGO2 dimerization is known; therefore, no positive control could be used.<sup>59</sup> Results are expressed as mean  $\pm$  SEM for  $n = 4$ . One-way ANOVA followed by Dunnett correction was performed to assess differences between treated and nontreated cells.

195 member of the G protein-coupled receptor (GPCR) family<sup>58</sup>  
 196 and proposed as a target receptor for TFF3 to mediate wound  
 197 healing.<sup>30,39</sup> We therefore pharmacologically characterized  
 198 TFF3(C<sup>57</sup>Acm) and TFF3 homodimer at CXCR4. We used  
 199 a chimeric  $G\alpha_{iq}$  protein to switch the pathway to the  $G\alpha_q$   
 200 signaling, which leads to the activation of the phospholipase  
 201 and allows measurement of CXCR4 activation through the  
 202 production of inositol 1 phosphate (IP1).<sup>61–63</sup> We measured  
 203 IP1 accumulation upon stimulation with TFF3 and TFF3  
 204 homodimer in fibroblast-like COS-7 cells transiently trans-  
 205 fected with CXCR4.<sup>58</sup> This is a competitive immunoassay,  
 206 based on the HTRF technology, where native IP1 produced by  
 207 cells compete with labeled IP1 (acceptor) for binding to anti-  
 208 IP1-cryptate (donor). The specific signal (i.e., Förster  
 209 resonance energy transfer, FRET) is inversely proportional to  
 210 the concentration of IP1 in the sample. The calculation of the  
 211 fluorescence ratio eliminates possible medium interferences.<sup>64</sup>  
 212 TFF3(C<sup>57</sup>Acm) and TFF3 homodimer were tested alone or  
 213 in combination with C-X-C motif chemokine 12 (CXCL12),  
 214 the natural CXCR4 ligand,<sup>58</sup> to assess TFF3's potential to act  
 215 as a CXCR4 agonist or antagonist. Neither TFF3(C<sup>57</sup>Acm)  
 216 nor TFF3 homodimer activated CXCR4 at concentrations up  
 217 to 10  $\mu$ M in contrast to the positive control CXCL12 (EC<sub>50</sub>  
 218 5.9 nM) (Figure 3D). The EC<sub>50</sub> of CXCL12 was also not

219 affected by TFF3 or TFF3 homodimer (up to 10  $\mu$ M), 219  
 220 suggesting that these peptides are also not antagonists (Figure 220  
 221 3D). 221

**TFF3 and TFF3 Homodimer Do Not Activate LINGO2** 222  
**in BRET Assay.** LINGO2 has also been put forward as a 223  
 224 potential TFF3 receptor.<sup>38</sup> We thus evaluated whether 224  
 225 TFF3(C<sup>57</sup>Acm) or TFF3 homodimer could disturb LINGO2 225  
 226 dimerization *via* a bioluminescence resonance energy transfer 226  
 227 (BRET) assay. This method allows the study of protein 227  
 228 interactions using energy transfer between a light-emitting 228  
 229 enzyme and a fluorescent acceptor protein.<sup>65</sup> LINGO2 fused 229  
 230 with *Renilla* luciferase (Rluc; protein donor) or yellow 230  
 231 fluorescent protein (YFP; protein acceptor) were co-expressed 231  
 232 in HEK-293 cells and BRET signal detected after adding the 232  
 233 luminescent substrate coelenterazine. We observed a strong 233  
 234 BRET signal under basal condition, demonstrating the capacity 234  
 235 of LINGO2 to form dimers, as already described.<sup>59</sup> We then 235  
 236 evaluated whether the TFF3 constructs could promote changes 236  
 237 of this basal BRET signal by inducing conformational change 237  
 238 within the dimers and/or change the dimerization state of 238  
 239 LINGO2. However, no statistically significant ( $p > 0.05$ ) 239  
 240 modification of BRET signal was observed following 240  
 241 stimulation of HEK-293 cells coexpressing LINGO2-YFP 241  
 242 and LINGO2-Rluc with TFF3(C<sup>57</sup>Acm) or TFF3 homodimer 242

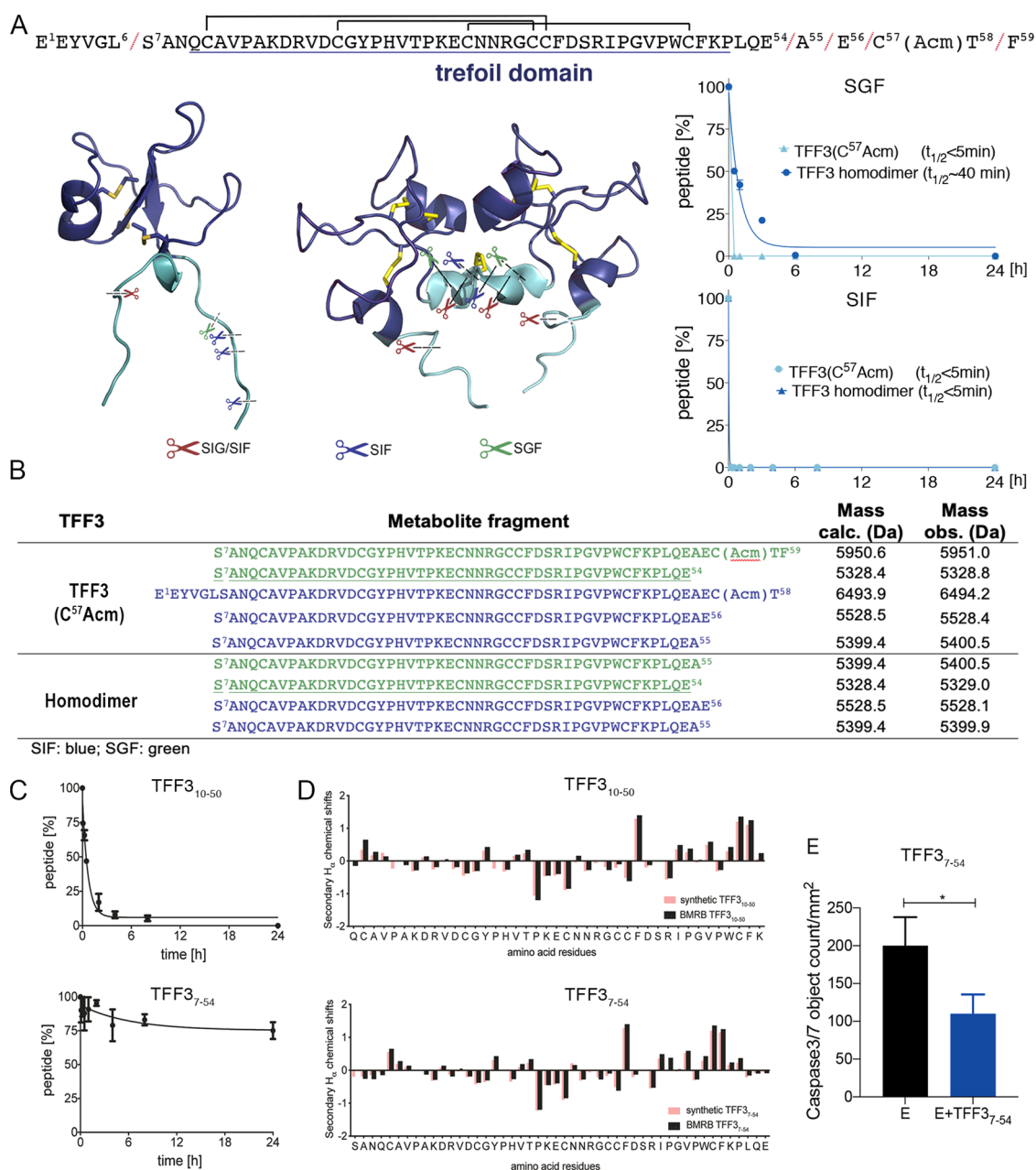


**Figure 4.** Identification and characterization of a stable and bioactive TFF3 metabolite (TFF3<sub>7-54</sub>). (A) The observed cleavage sites are highlighted in the three-dimensional structure and linear sequence of TFF3. The trefoil domain is underlined and displayed in blue in the sequence and NMR structure. (B) A table listing the observed fragments including their masses. The shortest stable metabolite (TFF3<sub>7-54</sub>) is underlined. (C) Intestinal stability of the trefoil domain TFF3<sub>10-50</sub> and the gut-stable metabolite TFF3<sub>7-54</sub>. (D) Comparison of the secondary H $\alpha$  chemical shifts of TFF3 (BMRB: 5771) and the trefoil domain TFF3<sub>10-50</sub> and TFF3 (BMRB: 5771) and the gut-stable metabolite TFF3<sub>7-54</sub>. Secondary H $\alpha$  chemical shifts were determined by subtracting the shifts observed in random coil peptides from the shifts determined from the 2D NMR analysis.<sup>57</sup> (E) Antiapoptotic effects of TFF3<sub>7-54</sub> on SH-SY5Y cells. E: etoposide. Etoposide and TFF3<sub>7-54</sub> were added at the same time. Caspase-3/7 activity was measured after 6 h. Results are expressed (mean  $\pm$  SEM) of  $n \geq 3$  independent experiments as the number of green fluorescent caspase-3/7 active objects generated by caspase-3/7 reagent added in media. One-way ANOVA followed by Dunnett correction was performed to assess differences between treated cells and etoposide only. \* $p < 0.05$ , \*\* $p < 0.01$ .

243 at any of the tested concentrations (0.1–10  $\mu\text{M}$ ) ( $p > 0.05$ )  
244 (Figure 3E).

245 **Gastrointestinal Stability Assays Revealed a Stable**  
246 **and Bioactive TFF3 Metabolite.** TFF3 is often considered  
247 metabolically stable due to its rigid disulfide-rich structure and  
248 function in the gut.<sup>3</sup> However, no systematic gut stability  
249 studies have been carried out and some reports indicate that  
250 TFF3 is not fully resistant to proteases. For example, only 15%  
251 of intravenously injected iodine-labeled TFF3 homodimer in

rats was recovered from urine after 24 h.<sup>26</sup> TFF3 homodimer  
252 was also degraded in the terminal parts of the large intestine<sup>27</sup>  
253 and truncated at the C-terminal Phe<sup>59</sup> in human saliva.<sup>28</sup> It was  
254 thus important to characterize TFF3's gastrointestinal stability  
255 in more detail, particularly considering that studies often rely  
256 on the use of sodium dodecyl sulfate (SDS) gels and  
257 antibodies to identify and characterize TFF3, where  
258 truncations can easily be missed.<sup>48,49,66</sup>  
259

260 We exposed TFF3(C<sup>57</sup>Acm) and TFF3 homodimer to  
261 simulated gastric fluid (SGF, containing pepsin, pH 1.3) and  
262 simulated intestinal fluid (SIF, containing pancreatic enzymes,  
263 pH 6.8), and monitored the mixture over 24 h by analytical  
264 RP-HPLC and MS. The N- and C-termini of TFF3 and its  
265 homodimer were readily truncated in both SGF and SIF  
266 (Figure 4A,B). In SGF, TFF3 was cleaved at Leu<sup>6</sup>/Ser<sup>7</sup>  
267 followed by cleavage at Glu<sup>54</sup>/Ala<sup>55</sup> ( $t_{1/2} < 5$  min). In SIF,  
268 TFF3 was cleaved first at Thr<sup>58</sup>/Phe<sup>59</sup> followed by cleavage at  
269 Leu<sup>6</sup>/Ser<sup>7</sup>, Glu<sup>56</sup>/Cys<sup>57</sup>, and Ala<sup>55</sup>/Glu<sup>56</sup> ( $t_{1/2} < 5$  min). TFF3  
270 homodimer, in both SGF ( $t_{1/2} \sim 40$  min) and SIF ( $t_{1/2} < 5$   
271 min), was first broken down to monomeric TFF3 through  
272 simultaneous cleavage at Leu<sup>6</sup> and Glu<sup>54</sup> or Ala<sup>55</sup>, eventually  
273 leading to the same metabolites as TFF3 (Figure 4B).  
274 Importantly, we identified two metabolites (TFF3<sub>7-54</sub> in SGF,  
275 and TFF3<sub>7-55</sub> in SIF) that remained stable even after 24 h  
276 (Figure 4B).

277 In certain physiological environments, disulfide bonds are  
278 prone to scrambling or reductive cleavage, thereby affecting  
279 peptide integrity.<sup>67</sup> Thus, we also evaluated the stability of the  
280 disulfide bonds of TFF3 in the presence of 10 equivalents of  
281 reduced glutathione (GSH) at pH 7 by time-course analytical  
282 RP-HPLC. No disulfide bond reduction or scrambling was  
283 observed for TFF3 or its homodimer (Figure S4) under these  
284 conditions. While this was expected for the relatively buried  
285 disulfide bonds within the trefoil domain (TFF3<sub>10-50</sub>), it  
286 highlights that also the disulfide bond outside of the trefoil  
287 domain is well protected.

288 We then synthesized the trefoil domain (TFF3<sub>10-50</sub>, single-  
289 chain assembly *via* Fmoc-SPPS) to investigate its gut stability.  
290 We acetylated the N-terminus (Gln<sup>10</sup>) of the trefoil domain to  
291 prevent the formation of pyroglutamic acid. TFF3<sub>10-50</sub> was  
292 stable in SGF for 24 h but exhibited low stability in SIF ( $t_{1/2} <$   
293 30 min) (Figure 4C). We incubated TFF3<sub>10-50</sub> with trypsin to  
294 identify some of the cleavage sites and observed cleavages at  
295 Lys<sup>16</sup>, Arg<sup>18</sup>, and Arg<sup>41</sup> and fragments Glu<sup>30</sup>-Arg<sup>34</sup> and Ile<sup>42</sup>-  
296 Lys<sup>50</sup> linked by a disulfide bond. A comparison of the NMR  
297 secondary  $\alpha$  chemical shifts of TFF3<sub>10-50</sub> with those of full-  
298 length TFF3 (BMRB: 5771) indicated that removal of the C-  
299 and N-terminal tails outside the trefoil domain did not change  
300 TFF3's overall domain structure (Figure 4D).

301 We also synthesized TFF3<sub>7-54</sub> (single-chain assembly *via*  
302 Fmoc-SPPS) to confirm the initial stability results and to  
303 elucidate whether the residues outside the trefoil domain  
304 (S<sup>7</sup>AN<sup>9</sup>, P<sup>51</sup>LQE<sup>54</sup>) were responsible for its greater stability.  
305 TFF3<sub>7-54</sub> was indeed stable in SGF and SIF with a half-life over  
306 24 h (Figure 4C);  $\sim 25\%$  degradation was observed in SIF  
307 within 24 h and MS analysis identified that cleavage mainly  
308 occurred near the C-terminus (Leu<sup>46</sup>/Gln<sup>47</sup> and Gln<sup>47</sup>/Glu<sup>48</sup>).  
309 Secondary  $\alpha$  chemical shifts of TFF3<sub>7-54</sub> confirmed that it  
310 had the same overall fold as full-length TFF3 (Figure 4D).  
311 TFF3<sub>7-54</sub> was also active in the anti-apoptosis assay, equivalent  
312 to TFF3 and TFF3 homodimer (Figure 4E). Taken together,  
313 these results suggest that the N- and C-terminal extended  
314 domain residues in TFF3<sub>7-54</sub> provide some steric protection  
315 against intestinal proteases and that the pharmacophore sits  
316 within the trefoil domain.

## 317 ■ DISCUSSION

318 Reliable synthetic access to TFF3 and its homodimer has been  
319 a long-standing challenge due to its length, difficult sequence  
320 segments, disulfide-rich character, and the presence of a  
321 seventh unpaired cysteine residue (Cys<sup>57</sup>) that enables homo-

or heterodimer formation.<sup>1,30</sup> Here, we achieved the chemical  
synthesis of the monomers TFF3(C<sup>57</sup>Acm) and TFF3, and the  
TFF3 homodimer (Figure 1). TFF3(C<sup>57</sup>Acm) is a valuable  
TFF3 analogue that cannot dimerize under physiological  
conditions, thereby enabling a more controlled study of the  
effects of monomeric vs homodimeric TFF3. The synthesis  
was achieved *via* a combination of Fmoc-SPPS and two-  
fragment NCL followed by an efficient oxidative folding step  
using well-defined conditions (Figure 1). Compared to other  
approaches (i.e., recombinant expression), our strategy has the  
advantage of providing full control over site-specific chemical  
modifications, being compatible with combinatorial ap-  
proaches and facilitating the incorporation of unnatural  
amino acids, bioconjugations handles, and reporter tags. This  
represents therefore an important new milestone for TFF3  
research, since it considerably expands ligand design options,  
important for molecular probe development, structure-activity  
relationship (SAR) studies, and therapeutic lead development.

TFF3's function has been associated with high metabolic  
stability to regulate gastrointestinal protection and repair,  
colorectal cancer development, and neuronal protection in the  
CNS.<sup>1,3,30</sup> However, its mechanism of action and target  
receptors remain speculative and have not been independently  
validated<sup>1,30</sup> and also the gastrointestinal stability has not been  
systematically investigated with some studies indicating that  
they are degraded.<sup>26,28</sup> The presumed high gastrointestinal  
stability of TFF3<sup>68-70</sup> would be an attractive feature from a  
peptide drug development point of view, since it could enable  
oral administration of TFF3-like drug candidates for the  
treatment of gastrointestinal disorders. With milligram  
quantities of TFF3 analogues at hand, we therefore  
investigated some of these aspects further to provide novel  
insights into TFF3's metabolic stability and mechanisms of  
action.

TFF3 and its homodimer were rapidly enzymatically  
truncated at both termini in the gastric (TFF3  $t_{1/2} < 5$  min;  
TFF3 homodimer  $t_{1/2} \sim 40$  min) as well as in the intestinal  
( $t_{1/2} < 5$  min) environment (Figure 4A), revealing a gut-stable  
metabolite (TFF3<sub>7-54</sub>) (Figure 4D). The slightly shorter trefoil  
domain (TFF3<sub>10-50</sub>) degraded in the intestinal environment  
( $t_{1/2} < 30$  min) (Figure 4C), highlighting that the residues  
S<sup>7</sup>AN<sup>9</sup> and P<sup>51</sup>LQE<sup>54</sup> outside the trefoil domain are important  
for the protection against gastrointestinal degradation. The  
metabolite TFF3<sub>7-54</sub> retained its overall three-dimensional  
structure, including its three loops and secondary motifs  
(Figure 4D), and displayed similar antiapoptotic activity as  
TFF3, suggesting that TFF3's pharmacophore sits within the  
trefoil domain. TFF3 homodimer has been reported to be  
more potent than TFF3 in promoting cell motility,<sup>31,32</sup> but  
considering the rapid degradation of the homodimer, it is  
remains questionable if it holds a major functional role in the  
gastrointestinal environment. This aligns with TFF3 being  
identified predominantly as a heterodimer (TFF3-FCGBP) in  
the colon, followed by the monomeric form, and only a small  
portion of TFF3 observed as a homodimer.<sup>29</sup> None of the  
metabolites have so far been reported, which is not surprising  
considering that the methods to identify and characterize  
TFF3 (i.e., SDS gels and antibodies) can easily miss terminal  
truncations.<sup>48,49</sup> The formation of heterodimers<sup>29</sup> and TFF3  
binding to mucins might furthermore protect against  
degradation.<sup>71</sup>

TFF3, TFF3 homodimer, and TFF3<sub>7-54</sub> all reduced  
apoptosis of SH-SY5Y, a human neuroblastoma cell line 384



385 (Figure 1), aligning well with reported antiapoptotic activity,  
386 including cerebral ischemia.<sup>22,33,72,73</sup> These antiapoptotic  
387 effects support TFF3's (neuro)protective role,<sup>1,33,72,73</sup> as well  
388 as its association as a tumor growth promoter in different  
389 cancers.<sup>8,74,75</sup> TFF3 and its homodimer did not display any  
390 cytotoxic or hemolytic effects, an important aspect for future  
391 therapeutic development of TFF3.

392 TFF3's interaction with CXCR4, a member of the GPCR  
393 family,<sup>58</sup> was proposed to mediate cell migration *via* an ERK1/  
394 2-independent signaling pathway.<sup>39</sup> This interaction was  
395 established in a human conjunctival epithelial cell line  
396 expressing CXCR4, where blockage of CXCR4 impaired  
397 TFF3-mediated cell migration.<sup>39</sup> While this suggests that  
398 CXCR4 is involved in the mechanism of action of TFF3, it did  
399 not provide evidence of direct TFF3-CXCR4 interaction. To  
400 validate this interaction, we tested TFF3 and TFF3  
401 homodimer in a well-established CXCR4 signaling  
402 assay,<sup>61–63</sup> demonstrating that they neither activated nor  
403 inhibited CXCR4 up to a concentration of 10  $\mu$ M (Figure 3D).  
404 These results correspond with another study that failed to co-  
405 localize TFF3 and CXCR4.<sup>38</sup>

406 The second putative TFF3 receptor that we investigated was  
407 LINGO2, which has recently been implicated with TFF3 in  
408 promoting protection against colitis *in vivo*.<sup>38</sup> Neither TFF3  
409 nor TFF3 homodimer displayed any effect on LINGO2  
410 dimerization, which was assessed by BRET (Figure 3E).<sup>59</sup> Due  
411 to the limited availability of functional LINGO2 bioassays, we  
412 cannot fully exclude that TFF3 does not signal through  
413 LINGO2 and we can only state that TFF3 does not interfere  
414 with dimerization.

## 415 ■ CONCLUSIONS

416 We have developed reliable synthetic strategies to produce  
417 TFF3 and analogues, which will markedly facilitate mechanistic  
418 and SAR studies as well as therapeutic development. We  
419 revealed a gut-stable TFF3 metabolite (TFF3<sub>7–54</sub>) that retained  
420 its bioactivity and demonstrated that TFF3, TFF3 homodimer,  
421 and the trefoil domain (TFF3<sub>10–50</sub>) are readily degraded in the  
422 gastrointestinal environment. We were not able to pharmaco-  
423 logically confirm a TFF3 signaling or interaction with CXCR4  
424 or LINGO2. The chemical synthesis of TFF3 and its  
425 homodimer as well as the discovery of the truncated bioactive  
426 TFF3 metabolite are important new developments for the field  
427 that provide new perspectives and opportunities for the design  
428 and development of advanced molecular probes and TFF3  
429 analogues facilitating both fundamental research as well as  
430 therapeutic development.

## 431 ■ EXPERIMENTAL SECTION

432 **Materials.** Fmoc-amino acids and Fmoc-Phe-Wang Tenta Gel  
433 resin (loading 0.7 mmol/g) were purchased from Iris Biotech GmbH  
434 (Marktredwitz, Germany). Rink amide Protide resin (loading 0.19  
435 mmol/g) and Oxyma Pure (ethyl cyanohydroxyiminoacetate) were  
436 obtained from CEM (Charlotte, NC). 2-Chlorotriptyl chloride resin  
437 (loading 2.0 mmol/g) was from Chem-Impex (Wood Dale). Pepsin  
438 from porcine gastric mucosa (3500–4500 units/mg solid), hydrazine  
439 hydrate and recombinant EGF (epidermal growth factor), and *N,N'*-  
440 diisopropylcarbodiimide (DIC) were from Sigma-Aldrich (Sydney,  
441 Australia). *N,N*-Dimethylformamide (DMF), pancreatin from porcine  
442 pancreas, trifluoroacetic acid (TFA), and diethyl ether were obtained  
443 from Chem-Supply (Gillman, Australia). Trypsin-EDTA 0.25%,  
444 Dulbecco's modified Eagle's medium (DMEM), and L-glutamine  
445 were from Invitrogen (Mulgrave, Australia). Fetal bovine serum  
446 (FBS) was from Scientifix (South Yarra, Australia). IncuCyte caspase-

3/7 green apoptosis reagent was purchased from Essenbioscience 447  
(Newark Close, U.K.). HEK-293 (ATCC CRL-1573) human 448  
embryonic kidney and SH-SY5Y cells were obtained from American 449  
Type Culture Collection (ATCC). Chitin beads were purchased from 450  
New England Biolabs GmbH (Frankfurt, Germany). IP-One Gq assay 451  
kit from CisBio (Codolet, France). Metafectene Pro was from Biontex 452  
Laboratories GmbH (Munich, Germany). pcDNA3.1 plasmid was 453  
kindly provided by Dr. Evi Kostenis, Rheinische Friedrich-Wilhelms- 454  
Universität, Bonn, Germany. All solvents were obtained in the highest 455  
available purity and used without further purification. All other 456  
chemicals were obtained from Sigma-Aldrich/Merck (Sydney, 457  
Australia) in the highest available purity. Recombinant monomeric 458  
and homodimeric human TFF3 produced in yeast were kindly 459  
provided by Dr. Lars Thim (Novo Nordisk A/S, Denmark). Human 460  
whole blood was obtained from the Australian Red Cross Blood 461  
Service. 462

**Ethics Statement.** Human ethics approval was obtained for use of 463  
human blood for hemolysis studies, from the University of 464  
Queensland Medical Research Ethics Committee (approval number 465  
2014000031). 466

**Peptide Synthesis. Preparation of 2-Chlorotriptyl Hydrazine** 467  
*Resin.* 2-Chlorotriptyl chloride resin was swelled in 50% DMF/DCM 468  
(v/v) for 30 min in a peptide synthesis vessel. The solution was 469  
drained, and the resin was treated with 10% hydrazine hydrate/DMF 470  
(v/v) for 30 min. After draining the solution, the resin was washed 471  
with DMF. Unreacted resin was capped with 5% MeOH/DMF (v/v) 472  
for 10 min and washed with DMF. The resin was directly used for the 473  
next coupling step. Resin loading was determined by quantitative 474  
Fmoc release. Briefly, 20% piperidine/DMF was added to a 10 mL 475  
volumetric flask containing 10 mg of dry resin and mixed for 30 min. 476  
A UV cuvette was filled with 100  $\mu$ L of the supernatant and diluted 477  
1:10 with 20% piperidine/DMF. The absorbance of the dibenzo- 478  
fulvene-piperidine adduct was measured using a UV spectrometer at 479  
301 nm. The resin loading (mmol/g) was then calculated using the 480  
following formula:  $A/(e \times d \times m) \times 106$ , where *A* is the absorbance, *e* 481  
is the extinction coefficient of dibenzofulvene adduct, *m* is the mass of 482  
resin (mg), and *d* is the dilution factor. 483

**Solid-Phase Peptide Synthesis.** NCL precursor peptide fragments 484  
of TFF3 (Cys<sup>57</sup>(Acm) and free Cys<sup>57</sup> forms) were synthesized on a 485  
Liberty Prime automatic synthesizer (CEM, Charlotte, NC) *via* 486  
Fmoc-SPPS on a 0.1 mmol scale. C-terminal fragment was 487  
synthesized using Fmoc-Phe-Wang (TFF3<sub>36–59</sub>) and the hydrazide 488  
fragment (TFF3<sub>1–35</sub>-NHNH<sub>2</sub>) on a freshly prepared 2-chlorotriptyl 489  
hydrazide resin. TFF3<sub>10–50</sub> and TFF3<sub>7–54</sub> were synthesized on a Rink 490  
amide protide resin. Amino acid side chains were protected as follows: 491  
Arg(2,2,4,6,7-pentamethyl-dihydrobenzofuran-5-sulfonyl), Asn/Gln- 492  
(trityl), Asp(O-3-methylpent-3-yl), Glu(*tert*-butyl ester (OtBu)), 493  
Cys(trityl or acetamidomethyl), His/Lys/Trp (*tert*-butyloxycarbonyl), 494  
and Ser/Thr/Tyr(*tert*-butyl (tBu)). Fmoc deprotection was per- 495  
formed using 25% pyrrolidine/DMF. Couplings (5 equiv) were 496  
carried out with DIC/Oxyma Pure at 105 °C. Fmoc-amino acid/ 497  
DIC/Oxyma (1:2:1). Upon completion of the peptide chain, the resin 498  
was washed with DCM/MeOH. Cleavage from the resin and 499  
simultaneous removal of side-chain-protecting groups was achieved 500  
by treatment with 90% trifluoroacetic acid (TFA)/5% triisopropylsil- 501  
lane (TIPS)/5% H<sub>2</sub>O at 25 °C for 90 min. Following cleavage, the 502  
solution was evaporated under a stream of N<sub>2</sub> and the products 503  
precipitated and were washed with cold Et<sub>2</sub>O and lyophilized in 50% 504  
acetonitrile (ACN)/0.1% TFA/H<sub>2</sub>O. The crude products were 505  
purified by preparative HPLC. 506

**Native Chemical Ligation.** Only fragments with purity > 90% were 507  
used for the NCL. The N-terminal fragment containing the hydrazide 508  
group (1.5 mM) was oxidized to an azide by dissolving the peptide in 509  
0.2 M sodium phosphate buffer solution containing 6 M Gn-HCl (pH 510  
3) and reacting it with NaNO<sub>2</sub> (10 equiv relative to the hydrazide 511  
fragment) for 15 min at –15 °C. During this step, the C-terminal 512  
fragment (1 mM) was dissolved in 0.2 M phosphate solution 513  
containing 6 M Gn-HCl and sodium 2-mercaptoethanesulfonate 514  
(MESNA; 100 equiv relative to the hydrazide fragment). The 515  
solutions containing the peptide segments were combined, and the 516



517 pH was carefully adjusted to 7.5 with NaOH. The reaction was  
518 monitored by analytical RP-HPLC and carried out for 24 h and  
519 purified by preparative RP-HPLC. TCEP (75 mM) was added to the  
520 reaction before RP-HPLC analysis and purification.

521 **Oxidative Folding.** Peptides were dissolved in a minimal amount of  
522 50% ACN/0.1% TFA/H<sub>2</sub>O and added to the oxidative buffer (0.1 M  
523 NH<sub>4</sub>HCO<sub>3</sub>) for a final concentration of 50  $\mu$ M, and the pH was  
524 adjusted to 8.5. Oxidation was monitored by analytical RP-HPLC and  
525 electrospray mass spectroscopy (ESI-MS). After complete oxidation,  
526 the pH was adjusted to 2 with neat TFA, filtered, and the peptide was  
527 purified by preparative RP-HPLC.

528 **Dimerization.** Folded monomeric TFF3 with the Cys<sup>57</sup> unpro-  
529 tected was dissolved in 50% ACN/0.1% TFA/H<sub>2</sub>O to a final  
530 concentration of 2.5 mM. Iodine (30 equiv) was added to accelerate  
531 the dimerization. After complete oxidation (2 min), the reaction was  
532 quenched with ascorbic acid and the peptide was purified by  
533 preparative RP-HPLC (~60% yield).

534 **RP-HPLC and LC-MS Methods.** Peptides were purified using either  
535 a preparative C<sub>18</sub> (Grace Vydac; 10  $\mu$ m, 2.2 cm ID  $\times$  250 mm, flow  
536 rate 15 mL/min) or C<sub>5</sub> (Phenomenex Luna; 10  $\mu$ m, 21.2 mm ID  $\times$   
537 250 mm, flow rate 15 mL/min) columns on a Waters 600 HPLC  
538 system (Waters Co., Milford, MA) using gradient of solvent A (0.05%  
539 TFA in water) and B (90% ACN/0.043% TFA/10% H<sub>2</sub>O) according  
540 to the peptide retention time observed by analytical RP-HPLC.  
541 TFF3<sub>1-35</sub> was purified using the C<sub>18</sub> preparative RP-HPLC column  
542 with a gradient of 10–40% B over 60 min (15% yield). TFF3<sub>36-59</sub>  
543 (20% yield) and reduced TFF3 (19% yield) were also purified on the  
544 C<sub>18</sub> preparative column with a gradient of 20–50% B over 60 min.  
545 Reduced TFF3 was washed with 10% B for 15 min before its  
546 purification to remove the salts from the ligation buffer. Folded TFF3  
547 was purified using the C<sub>5</sub> preparative RP-HPLC column with a  
548 gradient of 10–40% B over 60 min. The molecular mass of the  
549 fractions collected was analyzed by direct injection in an ESI-MS, and  
550 those with the desired mass were further analyzed by RP-HPLC and  
551 lyophilized. Peptides were analyzed by RP-HPLC using an analytical  
552 C<sub>3</sub> (Agilent Zorbax SB-C<sub>3</sub>, 5  $\mu$ m, 2.1 mm  $\times$  250 mm, 300 Å) or C<sub>18</sub>  
553 (Phenomenex Jupiter; 5  $\mu$ m, 2.1 mm  $\times$  250 mm, 300 Å) RP-HPLC  
554 column connected to a Shimadzu LC-20AT solvent delivery system  
555 equipped with an SIL-20AHT autoinjector and an SPD-20A  
556 Prominence ultraviolet–visible detector. Data were recorded and  
557 processed with the Shimadzu LabSolutions software (version 5.90). A  
558 linear gradient from 0 to 60% solvent B in 60 min was performed  
559 (solvent A 0.05% TFA in water and B 90% ACN/0.043% TFA/10%  
560 H<sub>2</sub>O), and absorbance data were collected at 214 nm to determine  
561 the purity of the final product. Only peptides with purity >95% were  
562 used for structural and biological analyses. The mass analysis of the  
563 peptides was performed using a Q-Star Pulsar mass spectrometer  
564 (SCIEX, Ontario, Canada) with a Series 1100 solvent delivery system  
565 equipped with an autoinjector (Agilent Technologies, Inc., Palo Alto,  
566 CA) and a Phenomenex Jupiter LC-MS C<sub>18</sub> column (90 Å, 4  $\mu$ m, 2  
567 mm  $\times$  250 mm). Linear gradients of 0.1% aqueous formic acid  
568 (solvent A) and 90% ACN/0.1% formic acid (solvent B) were  
569 employed at a flow rate of 250  $\mu$ L/min, and the column was  
570 maintained at 45 °C. The instrument was scanned in the *m/z* range of  
571 500–1800 Da. Data acquisition and processing were carried out using  
572 Analyst software v1.1 (SCIEX, Canada).

573 **Co-elution RP-HPLC Study of TFF3 Homodimer.** Synthetic and  
574 recombinant homodimeric TFF3 were co-injected at a 2:1  
575 (synthetic:recombinant) ratio and subjected to analytical RP-HPLC  
576 analysis using a 1% solvent B/min gradient on a C<sub>3</sub>-RP-HPLC  
577 column (Agilent Zorbax SB-C<sub>3</sub>, 5  $\mu$ m, 2.0 mm  $\times$  250 mm, 300 Å).

578 **In Vitro Stability Assay.** Simulated gastric fluid (SGF) was  
579 prepared by dissolving 20 mg of NaCl and 8 mg of pepsin in 70  
580  $\mu$ L of concentrated HCl (32%), and the volume was diluted to 10 mL  
581 with Milli-Q water (pH 1.3).<sup>76,77</sup> Simulated intestinal fluid (SIF) was  
582 prepared by dissolving 68 mg of KH<sub>2</sub>PO<sub>4</sub> in 500  $\mu$ L of Milli-Q water  
583 followed by the addition of 800  $\mu$ L of 0.2 M NaOH and 100 mg of  
584 porcine pancreatin, and the volume was adjusted to 10 mL with Milli-  
585 Q water (pH 6.8).<sup>76,77</sup> Peptide stock solution (1 mM; 15  $\mu$ L) was  
586 added to SGF (285  $\mu$ L) or SIF (285  $\mu$ L) and incubated at 37 °C.

587 Samples (30  $\mu$ L) from SGF and SIF were taken at 0, 5, 15, and 30  
588 min and 1, 2, 4, 8, and 24 h timepoints and subsequently quenched  
589 with 30  $\mu$ L of 0.2 M Na<sub>2</sub>CO<sub>3</sub> (SGF) or 30  $\mu$ L of 5% aqueous TFA  
590 (SIF). The samples were analyzed by analytical RP-HPLC (30  $\mu$ L)  
591 and/or LC-MS (20  $\mu$ L). The amount of peptide remaining was  
592 determined by measuring the peak area and expressing it as a % of the  
593 peak area at time 0. Peptide half-life (*t*<sub>1/2</sub>) was determined from the  
594 peptide degradation profiles using an exponential one-phase decay fit  
595 in Prism (version 7, GraphPad, La Jolla). LC-MS analysis was  
596 performed in a Q-Star Pulsar mass spectrometer (SCIEX, Ontario,  
597 Canada), and the raw data spectra were processed using the peptide  
598 reconstruction tool in the BioAnalyst software to identify the mass of  
599 the metabolites. The stability of the disulfide bonds was assessed  
600 through incubation of the peptides (10  $\mu$ M) with 10 equiv of reduced  
601 glutathione (GSH; 100  $\mu$ M) in sodium phosphate (50 mM) buffer at  
602 pH 7.2. Samples were taken at timepoints 0, 4, 8, and 24 h, quenched  
603 by adding 10% TFA, and analyzed by analytical RP-HPLC using an  
604 analytical C<sub>3</sub> column (Agilent Zorbax SB-C<sub>3</sub>, 5  $\mu$ m, 2.1 mm  $\times$  250  
605 mm, 300 Å).

606 **Circular Dichroism.** Stock solutions of the peptides were prepared  
607 in 50% ACN/H<sub>2</sub>O at 1 mM concentration. Peptide concentrations for  
608 CD analysis were 50  $\mu$ M in 10 mM sodium phosphate buffer (pH  
609 7.4). CD spectra were obtained on a Jasco J-810 spectropolarimeter  
610 (Easton, MD). All experiments were carried out in a 0.1 cm quartz  
611 cell with 250  $\mu$ L of sample at 25 °C and examined in the far-UV  
612 spectra region (185–260 nm), 20 nm/min scanning speed, 1 nm  
613 bandwidth, and 0.5 nm data pitch with five scans averaged for each  
614 sample. Blank subtraction was performed in the Spectra Management  
615 Software followed by smoothing using the Savitzky–Golay method.  
616 CD was reported as mean residue ellipticity ( $[\theta]$  (mdeg·cm<sup>2</sup>·dmol<sup>-1</sup>)  
617 = (100  $\times$   $\theta$ )/(*n*  $\times$  *c*  $\times$  *l*), where  $\theta$  is the raw output (mdeg), *n* is the  
618 number of peptide bonds, *c* is the concentration (M), and *l* is the  
619 cuvette path length (cm)).

620 **Nuclear Magnetic Resonance.** NMR spectra of peptides dissolved  
621 in 90% H<sub>2</sub>O/10% D<sub>2</sub>O (~1 mM) were recorded using a Bruker 600  
622 MHz Avance III NMR spectrometer equipped with a cryogenically  
623 cooled probe (cryoprobe) at 298 K. NOESY spectra was recorded  
624 with a mixing time of 200 ms and TOCSY with spin lock of 80 ms.  
625 Samples were internally referenced to water at 4.76 ppm. TopSpin  
626 (Bruker Biospin) and CCPNMR Analysis 2.4.1 (CCPN, University of  
627 Cambridge, Cambridge, U.K.) were used to process and assign the  
628 spectra, respectively. NOEs in the NOESY spectrum were manually  
629 picked and assigned. Secondary shifts were calculated by subtracting  
630 the random coil  $\alpha$  shift from the experimental  $\alpha$  shifts.<sup>57</sup>

631 **Antiapoptotic Assay.** SH-SY5Y cells were seeded (13–15  $\times$  10<sup>3</sup>  
632 cells/well) in 96-well microplates in DMEM with 10% (v/v) fetal calf  
633 serum (FCS; Gibco), 2 mM L-glutamine, and 100 units/mL  
634 penicillin/streptomycin. The media was replaced with low riboflavin,  
635 complete Ham's F12 medium with 10% (v/v) fetal calf serum, 2 mM  
636 L-glutamine, and 100 units/mL penicillin/streptomycin before the  
637 live-cell imaging. Cells were treated with the etoposide or the caspase-  
638 3 inhibitor or TFF3 monomer or homodimer in the presence of  
639 InCuCyte caspase-3/7 green apoptosis reagent. Data were acquired  
640 using an InCuCyte ZOOM instrument with standard scan type setting  
641 (4 images per well) every 2 h for 48 h.

642 **Cell Viability/Cytotoxicity Assays.** HEK-293 cells (5000 cells/  
643 well), suspended in DMEM supplemented with 10% FBS, were  
644 seeded into 384-well plates in a volume of 20  $\mu$ L. Monomeric and  
645 homodimeric TFF3 were added to the cells for a final concentration  
646 of 0.18–22.7  $\mu$ M. The cell plates were then incubated for 20 h at 37  
647 °C and 5% CO<sub>2</sub>. Tamoxifen was used as a positive control. After the  
648 incubation, 5  $\mu$ L of 100  $\mu$ M resazurin diluted in PBS was added to  
649 each well (final concentration ~11  $\mu$ M). The plates were then  
650 incubated for 3–4 h at 37 °C and 5% CO<sub>2</sub>. The fluorescence intensity  
651 (FI) was read using the TECAN Infinite M1000 PRO with  
652 excitation/emission 560/590 nm. Cytotoxicity or cell viability was  
653 calculated using the following equation: cell viability (%) = (FI<sub>sample</sub> -  
654 FI<sub>negative</sub>/FI<sub>untreated</sub> - FI<sub>negative</sub>)  $\times$  100. CC<sub>50</sub> (concentration at 50% cell  
655 viability) was calculated using a nonlinear regression analysis of log  
656 (concentration) vs normalized cell viability.

657 **Hemolysis Analysis.** Monomeric and homodimeric TFF3 were  
658 serially diluted twofold in 0.9% NaCl and seeded (25  $\mu$ L) in a 384-  
659 well polypropylene plate (0.2–25  $\mu$ M final concentration). Whole  
660 blood (10 mL/tube) was washed two to three times in three volumes  
661 of 0.9% NaCl, with centrifugation of 500g, with reduced deceleration,  
662 for 10 min between washes. The cells were counted using a Neubauer  
663 hemocytometer and then diluted to  $1 \times 10^8$ /mL in 0.9% NaCl. The  
664 cells (25  $\mu$ L/well) were added to the plates containing TFF3. Melittin  
665 was used as a positive control. The plates were sealed and then placed  
666 on a plate shaker for 10 min before being incubated for 1 h at 37 °C  
667 without shaking. Following incubation, the plates were centrifuged at  
668 1000g for 10 min to pellet cells and debris and then 25  $\mu$ L of the  
669 supernatant was transferred into a 384-well flat-bottom PS plate and  
670 absorbance (Abs) was read at 405 nm using a Tecan M1000 Pro  
671 monochromator plate reader. Percent hemolysis was calculated using  
672 the following equation: Hemolysis (%) =  $(\text{Abs}_{\text{sample}} - \text{Abs}_{\text{negative}} /$   
673  $\text{Abs}_{\text{positive}} - \text{Abs}_{\text{negative}}) \times 100$ . HC<sub>10</sub> and HC<sub>50</sub> (concentration at 10  
674 and 50% hemolysis, respectively) were calculated using nonlinear  
675 regression analysis of log (concentration) vs normalized hemolysis.

676 **Recombinant Expression and Purification of Human CXCL12.**  
677 The human CXCL12 (natural CXCR4 ligand) cDNA was cloned into  
678 the pTXB1 vector *via* Nde I and Sap I restriction sites. Generated  
679 plasmids were amplified in *E. coli* DH5 $\alpha$  in Luria-Bertani (LB)  
680 medium with 100  $\mu$ g/mL ampicillin and purified by the PureYield  
681 plasmid miniprep system (Promega GmbH, Mannheim, Germany).  
682 The correctness of the generated constructs was verified by Sanger  
683 dideoxy sequencing of the entire CXCL12 sequence. CXCL12 was  
684 expressed as fusion protein with a small intein domain from the  
685 *Mycobacterium xenopi gyrA* gene and a chitin-binding domain (CBD)  
686 in *E. coli* ER2566 in LB medium containing 100  $\mu$ g/mL ampicillin for  
687 5 h at 37 °C under shaking. Notably, the initial methionine, which is  
688 not present in the mature human protein, is not cleaved by *E. coli*;  
689 thus, the generated protein bears an additional N-terminal  
690 methionine.<sup>78</sup> After cell lysis, and inclusion body extraction and  
691 solubilization, fusion protein was purified on chitin beads and target  
692 protein was eluted with column buffer (20 mM HEPES, 500 mM  
693 NaCl, 1 mM EDTA, 3 M urea, pH 8 at 4 °C) containing 0.1 M DTT  
694 (dithiothreitol) and 0.2% Tween-20, according to the manufacturer's  
695 protocol. The protein thioester was subsequently hydrolyzed under  
696 basic conditions at pH 10 and 4 °C, and the target protein was  
697 purified by preparative RP-HPLC on a Phenomenex Jupiter C<sub>18</sub>  
698 column (300 Å, 5  $\mu$ m, 250 mm  $\times$  21.2 mm) using linear gradients of  
699 0.1% TFA/H<sub>2</sub>O and 0.08% TFA/ACN. The protein was restored in  
700 0.1 M NaH<sub>2</sub>PO<sub>4</sub>, 6 M guanidine hydrochloride, pH 6.0, and refolded  
701 by rapid dilution as described earlier.<sup>79</sup> Finally, refolded protein was  
702 isolated *via* preparative RP-HPLC on a Phenomenex Jupiter C<sub>18</sub>  
703 column (300 Å, 5  $\mu$ m, 250 mm  $\times$  21.2 mm) applying linear gradients  
704 of 0.1% TFA/H<sub>2</sub>O and 0.08% TFA/ACN. Identity and purity were  
705 determined with ESI-/MALDI-ToF mass spectrometry (Bruker  
706 Daltonik GmbH, Bremen, Germany) and analytical RP-HPLC,  
707 respectively. The protein concentration was determined by photo-  
708 metric measurement at 280 nm using the corresponding extinction  
709 coefficient.

710 **Inositol 1 Phosphate (IP1) Assay.** COS-7 cells (fibroblast-like cells  
711 from African green monkey) were transiently co-transfected with the  
712 CXCR4 C-terminally fused to eYFP in pVito2 vector and the  
713 untagged chimeric G protein  $G\alpha_{\Delta 6q14myr}$  in pcDNA3.1 plasmid using  
714 Metafectene Pro according to manufacturer's protocol. The cells were  
715 cultured in DMEM with higher glucose and supplemented with 10%  
716 FCS without any antibiotics at 37 °C and 5% CO<sub>2</sub> in 95% humidity.  
717 Cisbio IP-One G<sub>i</sub> assay kit was used according to previous description  
718 with minor modifications to measure activity.<sup>80</sup> Briefly, a standard  
719 curve was prepared in HBSS (Hanks' balanced salt solution) with 20  
720 mM LiCl to determine the linear range of the assay and 10 000 cells/  
721 well were cultured overnight in a 384-well flat white plate (Greiner  
722 Bio-one GmbH, Frickenhausen, Germany). TFF3 and its homodimer  
723 as well as CXCL12 were diluted in HBSS containing 20 mM LiCl.  
724 Stimulation was carried out for 1 h in triplicate at 37 °C.  
725 Subsequently, 3  $\mu$ L of IP1-d2 and 3  $\mu$ L of Ab-cryptate in lysis buffer  
726 were added to the wells and incubated on a tumbler for 60 min at 25

°C. Fluorescence was then measured at 620 and 665 nm and the  
HTRF (homogeneous time-resolved fluorescence) ratio (665/620  
nm) was calculated. Data analysis was performed with Prism (version  
7, GraphPad, La Jolla). Tested compounds were normalized to  
CXCL12 wild type, with the highest HTRF ratio set to 0% and the  
lowest HTRF ratio set to 100% response. For testing the agonistic  
activity TFF3 monomer, TFF3 homodimer and CXCL12 were  
individually used for stimulation in the concentration range of 10<sup>-12</sup>  
to 10<sup>-5</sup> M. Antagonistic activity was tested by stimulation of the cells  
with CXCL12 in the concentration range of 10<sup>-12</sup> to 10<sup>-5</sup> M after  
preincubation for 5 min with 1.5-fold concentrated TFF3 or its  
homodimer, respectively. The final concentration range of 10<sup>-12</sup> to  
10<sup>-5</sup> M to CXCL12 and 1 or 10  $\mu$ M to TFF3 monomer and  
homodimer was achieved by adding the compounds from a threefold  
concentrated stock solution.

**Bioluminescence Resonance Energy Transfer (BRET) Assay.**  
HEK-293 cells were cultured with 10% FBS at 37 °C and 5% CO<sub>2</sub>  
in DMEM for 72–96 h. The cells were passaged to collagen-  
pretreated 10 cm plates (1/200 dilution) and incubated at 37 °C and  
5% CO<sub>2</sub> overnight. The medium was changed 1 h before transfection.  
BRET assays were performed following transient transfection of the  
donor protein (LINGO2-RLuc) alone or with the acceptor protein  
(LINGO2-YFP) using the calcium phosphate method. The cells were  
rinsed twice with sterile PBS 1 $\times$  and incubated in fresh DMEM with  
10% FBS at 37 °C and 5% CO<sub>2</sub> overnight 1 day after transfection.  
Following 48 h of transfection, the medium was removed and the cells  
were rinsed twice with PBS 1 $\times$  and harvested with 10 mL of HBSS at  
25 °C. The cell suspension was seeded in quadruplets in a 96-well  
plate (~10 000 cells/well) in which different concentrations of  
monomeric and homodimeric TFF3 have been loaded. After 20 min  
incubation, the fluorescence was measured on a Mithras LB 940  
Multimode Microplate Reader (Berthold Technologies, Germany) to  
check if the peptides alone did not modify fluorescent emission of  
YFP following excitation at 485 nm and reading at 530 nm. Then,  
total luminescence was measured by following coelenterazine addition  
(final concentration 5  $\mu$ M). BRET signal was measured in four  
repeats and calculated by determining the emission ratio at 530/480  
nm on cells coexpressing donor and acceptor and by subtracting the  
emission background BRET signal ratio (530/480 nm) of cells  
expressing only donor protein, then multiplying by 1,000 to obtain  
results in millBRET units (mBU).

## ■ ASSOCIATED CONTENT

### Supporting Information

The Supporting Information is available free of charge at  
<https://pubs.acs.org/doi/10.1021/acs.jmedchem.1c00767>.

Oxidative folding of TFF3, analytical HPLC and high-  
resolution MS traces of TFF3(C<sup>57</sup>Acm) chemical  
synthesis, analytical HPLC profile of TFF3, and stability  
of TFF3 disulfide bonds (PDF)  
Molecular formula strings (CSV)

## ■ AUTHOR INFORMATION

### Corresponding Author

Markus Muttenthaler – Institute for Molecular Bioscience,  
The University of Queensland, Brisbane, QLD 4072,  
Australia; Institute of Biological Chemistry, Faculty of  
Chemistry, University of Vienna, 1090 Vienna, Austria;  
[orcid.org/0000-0003-1996-4646](https://orcid.org/0000-0003-1996-4646); Phone: (+43) 1 4277  
70515; Email: markus.muttenthaler@univie.ac.at

### Authors

Nayara Braga Emidio – Institute for Molecular Bioscience,  
The University of Queensland, Brisbane, QLD 4072,  
Australia; [orcid.org/0000-0001-7835-9636](https://orcid.org/0000-0001-7835-9636)  
Rajeshwari Meli – Institute of Biological Chemistry, Faculty of  
Chemistry, University of Vienna, 1090 Vienna, Austria



791 Hue N. T. Tran – Institute for Molecular Bioscience, The  
792 University of Queensland, Brisbane, QLD 4072, Australia;  
793 [orcid.org/0000-0001-5181-1899](https://orcid.org/0000-0001-5181-1899)

794 Heyeon Baik – Institute of Biological Chemistry, Faculty of  
795 Chemistry, University of Vienna, 1090 Vienna, Austria

796 Séverine Morisset-Lopez – Centre de Biophysique  
797 Moléculaire, CNRS, Unité Propre de Recherche 4301,  
798 Université d'Orléans, 45071 Orleans, France

799 Alysha G. Elliott – Institute for Molecular Bioscience, The  
800 University of Queensland, Brisbane, QLD 4072, Australia;  
801 [orcid.org/0000-0002-2983-0484](https://orcid.org/0000-0002-2983-0484)

802 Mark A. T. Blaskovich – Institute for Molecular Bioscience,  
803 The University of Queensland, Brisbane, QLD 4072,  
804 Australia; [orcid.org/0000-0001-9447-2292](https://orcid.org/0000-0001-9447-2292)

805 Sabrina Spiller – Institute of Biochemistry, Faculty of Life  
806 Sciences, Leipzig University, Leipzig 04103, Germany

807 Annette G. Beck-Sickinger – Institute of Biochemistry,  
808 Faculty of Life Sciences, Leipzig University, Leipzig 04103,  
809 Germany; [orcid.org/0000-0003-4560-8020](https://orcid.org/0000-0003-4560-8020)

810 Christina I. Schroeder – Institute for Molecular Bioscience,  
811 The University of Queensland, Brisbane, QLD 4072,  
812 Australia; Center for Cancer Research, National Cancer  
813 Institute, National Institutes of Health, Frederick, Maryland  
814 21702, United States; [orcid.org/0000-0002-6737-6374](https://orcid.org/0000-0002-6737-6374)

815 Complete contact information is available at:

816 <https://pubs.acs.org/10.1021/acs.jmedchem.1c00767>

#### 817 Author Contributions

818 N.B.E., C.I.S., and M.M. conceived the idea. N.B.E., M.M., and  
819 C.I.S. designed and supervised the experiments. N.B.E. and  
820 H.N.T.T. performed chemical synthesis and gastrointestinal  
821 stability assays. N.B.E. and C.I.S. performed structural analysis.  
822 N.B.E. and H.B. carried out migration, and R.M. performed  
823 anti-apoptosis assays. S.M.-L. performed the BRET assay.  
824 M.A.T.B. and A.G.E. carried out the cytotoxicity and hemolysis  
825 assays. S.S. performed and A.G.B.-S. supervised the CXCR4  
826 assays. N.B.E. analyzed the data and wrote the manuscript. All  
827 authors discussed the data, provided critical feedback, and  
828 commented on the manuscript. The manuscript was written  
829 through contributions of all authors. All authors have given  
830 approval to the final version of the manuscript.

#### 831 Notes

832 The authors declare no competing financial interest.

#### 833 ACKNOWLEDGMENTS

834 M.M. was supported by the European Research Council  
835 (ERC) under the European Union's Horizon 2020 research  
836 and innovation program (714366) and by the Australian  
837 Research Council (ARC) (DE150100784, DP190101667).  
838 C.I.S. was an ARC Future Fellow (FT160100055). R.M. was  
839 supported by the Austrian Science Fund (FWF) and Hertha  
840 Firnberg program (T948-B27). N.B.E. was supported by the  
841 University of Queensland International Postgraduate Scholar-  
842 ship. The authors thank Janet Reid and CO-ADD (the  
843 Community for Open Antimicrobial Drug Discovery), funded  
844 by the Wellcome Trust (Strategic Award 104797/Z/14/Z)  
845 and the University of Queensland, for the cytotoxicity and  
846 hemolysis assays. They thank Dr. Lars Thim (Novo Nordisk  
847 A/S) for providing the recombinant TFF3, and Prof. Paul  
848 Alewood (The University of Queensland) for his overall  
849 support of this work.

#### 850 ABBREVIATIONS

BRET, bioluminescence resonance energy transfer; CD, 851  
circular dichroism; CXCL12, C-X-C motif chemokine 12; 852  
CXCR4, chemokine receptor type 4; CNS, central nervous 853  
system; EGFR, enhanced epidermal growth factor receptor; 854  
FCGBP, Fc fragment of IgG Fc binding protein; Fmoc-SPPS, 855  
9-fluorenylmethyloxycarbonyl-solid-phase peptide synthesis; 856  
GSH, reduced glutathione; HEK-293, human embryonic 857  
kidney 293; IBD, inflammatory bowel diseases; LINGO2, 858  
leucine-rich repeat receptor and nogo-interacting protein 2; 859  
MESNA, sodium 2-mercaptoethanesulfonate; NOESY, nuclear 860  
Overhauser effect spectroscopy; NMR, nuclear magnetic 861  
resonance; SGF, simulated gastric fluid; SIF, simulated 862  
intestinal fluid; TOCSY, total correlation spectroscopy 863

#### 864 REFERENCES

- (1) Braga Emidio, N.; Brierley, S. M.; Schroeder, C. I.; Muttenthaler, 865  
M. Structure, function, and therapeutic potential of the trefoil factor 866  
family in the gastrointestinal tract. *ACS Pharmacol. Transl. Sci.* **2020**, 867  
3, 583–597. 868
- (2) Taupin, D.; Podolsky, D. K. Trefoil factors: Initiators of mucosal 869  
healing. *Nat. Rev. Mol. Cell Biol.* **2003**, 4, 721. 870
- (3) Thim, L.; May, F. E. B. Structure of mammalian trefoil factors 871  
and functional insights. *Cell. Mol. Life Sci.* **2005**, 62, 2956–2973. 872
- (4) Aihara, E.; Engevik, K. A.; Montrose, M. H. Trefoil factor 873  
peptides and gastrointestinal function. *Annu. Rev. Physiol.* **2017**, 79, 874  
357–380. 875
- (5) Dignass, A.; Lynch-Devaney, K.; Kindon, H.; Thim, L.; 876  
Podolsky, D. K. Trefoil peptides promote epithelial migration through 877  
a transforming growth factor beta-independent pathway. *J. Clin. Invest.* 878  
**1994**, 94, 376–383. 879
- (6) Hoffmann, W.; Jagla, W.; Wiede, A. Molecular medicine of TFF- 880  
peptides: from gut to brain. *Histol. Histopathol.* **2001**, 16, 319–334. 881
- (7) Schwarz, H.; Jagla, W.; Wiede, A.; Hoffmann, W. Ultrastructural 882  
co-localization of TFF3-peptide and oxytocin in the neural lobe of the 883  
porcine pituitary. *Cell Tissue Res.* **2001**, 305, 411–416. 884
- (8) Perry, J. K.; Kannan, N.; Grandison, P. M.; Mitchell, M. D.; 885  
Lobie, P. E. Are trefoil factors oncogenic? *Trends Endocrinol. Metab.* 886  
**2008**, 19, 74–81. 887
- (9) Jahan, R.; Shah, A.; Kisling, S. G.; Macha, M. A.; Thayer, S.; 888  
Batra, S. K.; Kaur, S. Odyssey of trefoil factors in cancer: diagnostic 889  
and therapeutic implications. *BBA, Biochim. Biophys. Acta, Rev. Cancer* 890  
**2020**, No. 188362. 891
- (10) Madsen, J.; Nielsen, O.; Tormoe, I.; Thim, L.; Holmskov, U. 892  
Tissue localization of human trefoil factors 1, 2, and 3. *J. Histochem.* 893  
*Cytochem.* **2007**, 55, 505–513. 894
- (11) Mashimo, H.; Wu, D. C.; Podolsky, D. K.; Fishman, M. C. 895  
Impaired defense of intestinal mucosa in mice lacking intestinal trefoil 896  
factor. *Science* **1996**, 274, 262–265. 897
- (12) Farrell, J. J.; Taupin, D.; Koh, T. J.; Chen, D.; Zhao, C. M.; 898  
Podolsky, D. K.; Wang, T. C. TFF2/SP-deficient mice show 899  
decreased gastric proliferation, increased acid secretion, and increased 900  
susceptibility to NSAID injury. *J. Clin. Invest.* **2002**, 109, 193–204. 901
- (13) Guppy, N. J.; El-Bahrawy, M. E.; Kocher, H. M.; Fritsch, K.; 902  
Qureshi, Y. A.; Poulson, R.; Jeffery, R. E.; Wright, N. A.; Otto, W. R.; 903  
Alison, M. R. Trefoil factor family peptides in normal and diseased 904  
human pancreas. *Pancreas* **2012**, 41, 888–896. 905
- (14) Longman, R. J.; Douthwaite, J.; Sylvester, P. A.; Poulson, R.; 906  
Corfield, A. P.; Thomas, M. G.; Wright, N. A. Coordinated 907  
localisation of mucins and trefoil peptides in the ulcer associated 908  
cell lineage and the gastrointestinal mucosa. *Gut* **2000**, 47, 792–800. 909
- (15) Alison, M. R.; Chinery, R.; Poulson, R.; Ashwood, P.; 910  
Longcroft, J. M.; Wright, N. A. Experimental ulceration leads to 911  
sequential expression of spasmolytic polypeptide, intestinal trefoil 912  
factor, epidermal growth-factor and transforming growth-factor-alpha 913  
messenger-RNAs in rat stomach. *J. Pathol.* **1995**, 175, 405–414. 914



- 915 (16) Aamann, L.; Vestergaard, E. M.; Groenbaek, H. Trefoil factors  
916 in inflammatory bowel disease. *World J. Gastroenterol.* **2014**, *20*,  
917 3223–3230.
- 918 (17) Furuta, G. T.; Turner, J. R.; Taylor, C. T.; Hershberg, R. M.;  
919 Comerford, K.; Narravula, S.; Podolsky, D. K.; Colgan, S. P. Hypoxia-  
920 inducible factor 1-dependent induction of intestinal trefoil factor  
921 protects barrier function during hypoxia. *J. Exp. Med.* **2001**, *193*,  
922 1027–1034.
- 923 (18) Arnold, P.; Rickert, U.; Helmers, A. K.; Spreu, J.;  
924 Schneppenheim, J.; Lucius, R. Trefoil factor 3 shows anti-  
925 inflammatory effects on activated microglia. *Cell Tissue Res.* **2016**,  
926 *365*, 3–11.
- 927 (19) Shi, H. S.; Yin, X.; Song, L.; Guo, Q. J.; Luo, X. H.  
928 Neuropeptide Trefoil factor 3 improves learning and retention of  
929 novel object recognition memory in mice. *Behav. Brain Res.* **2012**,  
930 *227*, 265–269.
- 931 (20) Shi, H. S.; Zhu, W. L.; Liu, J. F.; Luo, Y. X.; Si, J. J.; Wang, S. J.;  
932 Xue, Y. X.; Ding, Z. B.; Shi, J.; Lu, L. PI3K/Akt signaling pathway in  
933 the basolateral amygdala mediates the rapid antidepressant-like effects  
934 of trefoil factor 3. *Neuropsychopharmacology* **2012**, *37*, 2671–2683.
- 935 (21) Li, J. L.; Luo, Y. X.; Zhang, R. X.; Shi, H. S.; Zhu, W. L.; Shi, J.  
936 Neuropeptide trefoil factor 3 reverses depressive-like behaviors by  
937 activation of BDNF-ERK-CREB signaling in olfactory bulbectomized  
938 rats. *Int. J. Mol. Sci.* **2015**, *16*, 28386–28400.
- 939 (22) Liu, S. Q.; Roberts, D.; Zhang, B.; Ren, Y. P.; Zhang, L. Q.; Wu,  
940 Y. H. Trefoil Factor 3 as an Endocrine Neuroprotective Factor from  
941 the Liver in Experimental Cerebral Ischemia/Reperfusion Injury.  
942 *PLoS One* **2013**, *8*, e77732.
- 943 (23) Hoffmann, W. TFF Peptides. In *Handbook of Biologically Active*  
944 *Peptides*, Second ed.; Academic Press, 2013; pp 1338–1345.
- 945 (24) Lemercinier, X.; Muskett, F. W.; Cheeseman, B.; McIntosh, P.  
946 B.; Thim, L.; Carr, M. D. High-resolution solution structure of human  
947 intestinal trefoil factor and functional insights from detailed structural  
948 comparisons with the other members of the trefoil family of  
949 mammalian cell motility factors. *Biochemistry* **2001**, *40*, 9552–9559.
- 950 (25) Taupin, D.; Podolsky, D. K. Trefoil factors: initiators of  
951 mucosal healing. *Nat. Rev. Mol. Cell. Biol.* **2003**, *4*, 721–732.
- 952 (26) Poulsen, S. S.; Thulesen, J.; Hartmann, B.; Kissow, H. L.; Nexø,  
953 E.; Thim, L. Injected TFF1 and TFF3 bind to TFF2-immunoreactive  
954 cells in the gastrointestinal tract in rats. *Regul. Pept.* **2003**, *115*, 91–99.
- 955 (27) Kjellef, S.; Vestergaard, E. M.; Nexø, E.; Thygesen, P.; Ehoj, M.  
956 S.; Jeppesen, P. B.; Thim, L.; Pedersen, N. B.; Poulsen, S. S.  
957 Pharmacokinetics of trefoil peptides and their stability in gastro-  
958 intestinal contents. *Peptides* **2007**, *28*, 1197–1206.
- 959 (28) Houben, T.; Harder, S.; Schlüter, H.; Kalbacher, H.; Hoffmann,  
960 W. Different forms of TFF3 in the human saliva: heterodimerization  
961 with IgG Fc binding protein (FCGBP). *Int. J. Mol. Sci.* **2019**, *20*, 5000.
- 962 (29) Albert, T. K.; Laubinger, W.; Müller, S.; Hanisch, F. G.;  
963 Kalinski, T.; Meyer, F.; Hoffmann, W. Human intestinal TFF3 forms  
964 disulfide-linked heteromers with the mucus-associated FCGBP  
965 protein and is released by hydrogen sulfide. *J. Proteome Res.* **2010**,  
966 *9*, 3108–3117.
- 967 (30) Braga Emidio, N.; Hoffmann, W.; Brierley, S. M.; Muttenthaler,  
968 M. Trefoil factor family: unresolved questions and clinical  
969 perspectives. *Trends Biochem. Sci.* **2019**, *44*, 387–390.
- 970 (31) Marchbank, T.; Westley, B. R.; May, F. E. B.; Calnan, D. P.;  
971 Playford, R. J. Dimerization of human pS2 (TFF1) plays a key role in  
972 its protective/healing effects. *J. Pathol.* **1998**, *185*, 153–158.
- 973 (32) Poulsen, S. S.; Kissow, H.; Hare, K.; Hartmann, B.; Thim, L.  
974 Luminal and parenteral TFF2 and TFF3 dimer and monomer in two  
975 models of experimental colitis in the rat. *Regul. Pept.* **2005**, *126*, 163–  
976 171.
- 977 (33) Taupin, D. R.; Kinoshita, K.; Podolsky, D. K. Intestinal trefoil  
978 factor confers colonic epithelial resistance to apoptosis. *Proc. Natl.*  
979 *Acad. Sci. U.S.A.* **2000**, *97*, 799–804.
- 980 (34) Chen, Y. H.; Lu, Y.; De Plaen, I. G.; Wang, L. Y.; Tan, X. D.  
981 Transcription factor NF- $\kappa$ B signals antianoxic function of trefoil  
982 factor 3 on intestinal epithelial cells. *Biochem. Biophys. Res. Commun.*  
983 **2000**, *274*, 576–582.
- (35) Chinery, R.; Playford, R. J. Combined intestinal trefoil factor  
and epidermal growth-factor is prophylactic against indomethacin-  
induced gastric damage in the rat. *Clin. Sci.* **1995**, *88*, 401–403.
- (36) Dürer, U.; Hartig, R.; Bang, S.; Thim, L.; Hoffmann, W. TFF3  
and EGF induce different migration patterns of intestinal epithelial  
cells in vitro and trigger increased internalization of E-cadherin. *Cell*  
*Physiol. Biochem.* **2007**, *20*, 329–346.
- (37) Duraj-Thatte, A. M.; Praveschotinunt, P.; Nash, T. R.; Ward, F.  
R.; Joshi, N. S. Modulating bacterial and gut mucosal interactions with  
engineered biofilm matrix proteins. *Sci. Rep.* **2018**, *8*, No. 3475.
- (38) Belle, N. M.; Ji, Y.; Herbine, K.; Wei, Y.; Park, J.; Zullo, K.;  
Hung, L. Y.; Srivatsa, S.; Young, T.; Oniskey, T.; Pastore, C.; Nieves,  
W.; Somsouk, M.; Herbert, D. R. TFF3 interacts with LINGO2 to  
regulate EGFR activation for protection against colitis and gastro-  
intestinal helminths. *Nat. Commun.* **2019**, *10*, No. 4408.
- (39) Dieckow, J.; Brandt, W.; Hattermann, K.; Mentlein, R.; Schob,  
S.; Schulze, U.; Ackermann, P.; Sel, S.; Paulsen Friedrich, P. CXCR4  
and CXCR7 mediate TFF3-induced cell migration independently  
from the ERK1/2 signaling pathway. *Invest. Ophthalmol. Visual Sci.*  
**2016**, *57*, S6–S6.
- (40) Vandembroucke, K.; Hans, W.; Van Huysse, J.; Neiryneck, S.;  
Demetter, P.; Remaut, E.; Rottiers, P.; Steidler, L. Active delivery of  
trefoil factors by genetically modified *Lactococcus lactis* prevents and  
heals acute colitis in mice. *Gastroenterology* **2004**, *127*, 502–513.
- (41) Tran, C. P.; Cook, G. A.; Yeomans, N. D.; Thim, L.; Giraud, A.  
S. Trefoil peptide TFF2 (spasmolytic polypeptide) potently  
accelerates healing and reduces inflammation in a rat model of  
colitis. *Gut* **1999**, *44*, 636–642.
- (42) Babyatsky, M. W.; deBeaumont, M.; Thim, L.; Podolsky, D. K.  
Oral trefoil peptides protect against ethanol- and indomethacin-  
induced gastric injury in rats. *Gastroenterology* **1996**, *110*, 489–497.
- (43) Mahmood, A.; Melley, L.; Fitzgerald, A. J.; Ghosh, S.; Playford,  
R. J. Trial of trefoil factor 3 enemas, in combination with oral 5-  
aminosalicylic acid, for the treatment of mild-to-moderate left-sided  
ulcerative colitis. *Aliment. Pharmacol. Ther.* **2005**, *21*, 1357–1364.
- (44) Peterson, D. E.; Barker, N. P.; Akhmadullina, L. I.; Rodionova,  
I.; Sherman, N. S.; Davidenko, I. S.; Rakovskaya, G. N.; Gotovkin, E.  
A.; Shinkarev, S. A.; Kopp, M. V.; Kulikov, E. P.; Moiseyenko, V. M.;  
Gertner, J. M.; Firsov, I.; Tuleneva, T.; Yarosh, A.; Woon, C. W.  
Phase II, randomized, double-blind, placebo-controlled study of  
recombinant human intestinal trefoil factor oral spray for prevention  
of oral mucositis in patients with colorectal cancer who are receiving  
fluorouracil-based chemotherapy. *J. Clin. Oncol.* **2009**, *27*, 4333–  
4338.
- (45) Thim, L.; Woldike, H. F.; Nielsen, P. F.; Christensen, M.;  
Lynchdevaney, K.; Podolsky, D. K. Characterization of human and rat  
intestinal trefoil factor produced in yeast. *Biochemistry* **1995**, *34*,  
4757–4764.
- (46) Wang, H. B.; Tong, Y. P.; Fang, M.; Ru, B. G. High-level  
expression of human TFF3 in *Escherichia coli*. *Peptides* **2005**, *26*,  
1213–1218.
- (47) Le, J.; Zhang, D. Y.; Zhao, Y.; Qiu, W.; Wang, P.; Sun, Y. ITF  
promotes migration of intestinal epithelial cells through crosstalk  
between the ERK and JAK/STAT3 pathways. *Sci. Rep.* **2016**, *6*,  
No. 33014.
- (48) Barrera, G. J.; Sanchez, G.; Gonzalez, J. E. Trefoil factor 3  
isolated from human breast milk downregulates cytokines (IL8 and  
IL6) and promotes human beta defensin (hBD2 and hBD4)  
expression in intestinal epithelial cells HT-29. *Bosnian J. Basic. Med.*  
*Sci.* **2012**, *12*, 256–264.
- (49) Yu, K.; Jiang, S. F.; Lin, M. F.; Wu, J. B.; Lin, J. Extraction and  
purification of biologically active intestinal trefoil factor from human  
meconium. *Lab. Invest.* **2004**, *84*, 390–392.
- (50) Zheng, J. S.; Tang, S.; Qi, Y. K.; Wang, Z. P.; Liu, L. Chemical  
synthesis of proteins using peptide hydrazides as thioester surrogates.  
*Nat. Protoc.* **2013**, *8*, 2483–2495.
- (51) Luo, H. B.; Cao, M. Y.; Newell, K.; Afdahl, C.; Wang, J.; Wang,  
W. K.; Li, Y. L. Double-peak elution profile of a monoclonal antibody  
in cation exchange chromatography is caused by histidine-

- 1053 protonation-based charge variants. *J. Chromatogr. A* **2015**, *1424*, 92–  
1054 101.
- 1055 (52) Cardoso, F. C.; Dekan, Z.; Smith, J. J.; Deuis, J. R.; Vetter, I.;  
1056 Herzig, V.; Alewood, P. F.; King, G. F.; Lewis, R. J. Modulatory  
1057 features of the novel spider toxin mu-TRTX-Df1a isolated from the  
1058 venom of the spider *Davus fasciatus*. *Br. J. Pharmacol.* **2017**, *174*,  
1059 2528–2544.
- 1060 (53) Wingerd, J. S.; Mozar, C. A.; Ussing, C. A.; Murali, S. S.; Chin,  
1061 Y. K.; Cristofori-Armstrong, B.; Durek, T.; Gilchrist, J.; Vaughan, C.  
1062 W.; Bosmans, F.; Adams, D. J.; Lewis, R. J.; Alewood, P. F.; Mobli,  
1063 M.; Christie, M. J.; Rash, L. D. The tarantula toxin beta/delta-TRTX-  
1064 Pre1a highlights the importance of the S1-S2 voltage-sensor region for  
1065 sodium channel subtype selectivity. *Sci. Rep.* **2017**, *7*, No. 974.
- 1066 (54) Takahashi, H.; Kim, J. I.; Min, H. J.; Sato, K.; Swartz, K. J.;  
1067 Shimada, I. Solution structure of hanatoxin1, a gating modifier of  
1068 voltage-dependent K(+) channels: common surface features of gating  
1069 modifier toxins. *J. Mol. Biol.* **2000**, *297*, 771–780.
- 1070 (55) Braga Emidio, N.; Baik, H.; Lee, D.; Sturmer, R.; Heuer, J.;  
1071 Elliott, A. G.; Blaskovich, M. A. T.; Haupenthal, K.; Tegtmeyer, N.;  
1072 Hoffmann, W.; Schroeder, C. I.; Muttenthaler, M. Chemical synthesis  
1073 of human trefoil factor 1 (TFF1) and its homodimer provides novel  
1074 insights into their mechanisms of action. *Chem. Commun.* **2020**, *56*,  
1075 6420–6423.
- 1076 (56) Muskett, F. W.; May, F. E. B.; Westley, B. R.; Feeney, J.  
1077 Solution structure of the disulfide-linked dimer of human intestinal  
1078 trefoil factor (TFF3): the intermolecular orientation and interactions  
1079 are markedly different from those of other dimeric trefoil protein.  
1080 *Biochemistry* **2003**, *42*, 15139–15147.
- 1081 (57) Wishart, D. S.; Bigam, C. G.; Holm, A.; Hodges, R. S.; Sykes, B.  
1082 D. 1H, 13C and 15N random coil NMR chemical shifts of the  
1083 common amino acids. I. Investigations of nearest-neighbor effects. *J.*  
1084 *Biomol. NMR* **1995**, *5*, 67–81.
- 1085 (58) Lefrançois, M.; Lefebvre, M. R.; Saint-Onge, G.; Boulais, P. E.;  
1086 Lamothe, S.; Leduc, R.; Lavigne, P.; Heveker, N.; Escher, E. Agonists  
1087 for the Chemokine Receptor CXCR4. *ACS Med. Chem. Lett.* **2011**, *2*,  
1088 597–602.
- 1089 (59) Guillemain, A.; Laouarem, Y.; Cobret, L.; Stefok, D.; Chen, W.  
1090 Y.; Bloch, S.; Zahaf, A.; Blot, L.; Reverchon, F.; Normand, T.;  
1091 Decoville, M.; Grillon, C.; Traiffort, E.; Morisset-Lopez, S. LINGO  
1092 family receptors are differentially expressed in the mouse brain and  
1093 form native multimeric complexes. *FASEB J.* **2020**, *34*, 13641–13653.
- 1094 (60) Czekanska, E. M. Assessment of cell proliferation with  
1095 resazurin-based fluorescent dye. In *Methods in Molecular Biology*;  
1096 Humana Press, 2011; Vol. 740, pp 27–32.
- 1097 (61) Kostenis, E. Potentiation of GPCR-signaling via membrane  
1098 targeting of G protein alpha subunits. *J. Recept. Signal Transduction*  
1099 *Res.* **2002**, *22*, 267–281.
- 1100 (62) Berridge, M. J. Rapid accumulation of inositol trisphosphate  
1101 reveals that agonists hydrolyze polyphosphoinositides instead of  
1102 phosphatidylinositol. *Biochem. J.* **1983**, *212*, 849–858.
- 1103 (63) Berridge, M. J.; Dawson, R. M. C.; Downes, C. P.; Heslop, J. P.;  
1104 Irvine, R. F. Changes in the levels of inositol phosphates after agonist-  
1105 dependent hydrolysis of membrane phosphoinositides. *Biochem. J.*  
1106 **1983**, *212*, 473–482.
- 1107 (64) Degorce, F.; Card, A.; Soh, S.; Trinquet, E.; Knapik, G. P.; Xie,  
1108 B. HTRF: A technology tailored for drug discovery - a review of  
1109 theoretical aspects and recent applications. *Curr. Chem. Genomics*  
1110 **2009**, *3*, 22–32.
- 1111 (65) El Khamlichi, C.; Reverchon-Assadi, F.; Hervouet-Coste, N.;  
1112 Blot, L.; Reiter, E.; Morisset-Lopez, S. Bioluminescence resonance  
1113 energy transfer as a method to study protein-protein interactions:  
1114 application to G protein coupled receptor biology. *Molecules* **2019**, *24*,  
1115 537.
- 1116 (66) Qi, G. F.; Li, J. J.; Wang, S. Y.; Xin, S. S.; Du, P.; Zhang, Q. Y.;  
1117 Zhao, X. Y. A chimeric peptide of intestinal trefoil factor containing  
1118 cholesteryl ester transfer protein B cell epitope significantly inhibits  
1119 atherosclerosis in rabbits after oral administration. *Peptides* **2011**, *32*,  
1120 790–796.
- (67) Räder, A. F. B.; Weinmuller, M.; Reichart, F.; Schumacher-  
Klinger, A.; Merzbach, S.; Gilon, C.; Hoffman, A.; Kessler, H. Orally  
active peptides: is there a magic bullet? *Angew. Chem., Int. Ed.* **2018**,  
*57*, 14414–14438.
- (68) Jørgensen, K. H.; Thim, L.; Jacobsen, H. E. Pancreatic  
spasmolytic polypeptide (PSP): I. preparation and initial chemical  
characterization of a new polypeptide from porcine pancreas. *Regul.*  
*Pept.* **1982**, *3*, 207–219.
- (69) Playford, R. J.; Marchbank, T.; Chinery, R.; Evison, R.;  
Pignatelli, M.; Boulton, R. A.; Thim, L.; Hanby, A. M. Human  
spasmolytic polypeptide is a cytoprotective agent that stimulates cell-  
migration. *Gastroenterology* **1995**, *108*, 108–116.
- (70) Sun, Y.; Peng, X.; Zhang, Y.; Lv, S. J.; Wu, W.; Wang, S. L.  
Stability and biological activity of human intestinal trefoil factor  
produced by *Pichia pastoris*. *Protein Pept. Lett.* **2008**, *15*, 255–259.
- (71) Yu, H.; He, Y.; Zhang, X.; Peng, Z.; Yang, Y.; Zhu, R.; Bai, J.;  
Tian, Y.; Li, X.; Chen, W.; Fang, D.; Wang, R. The rat IgGFcγBP and  
MUC2 C-terminal domains and TFF3 in two intestinal mucus layers  
bind together by covalent interaction. *PLoS One* **2011**, *6*, No. e20334.
- (72) Kinoshita, K.; Taupin, D. R.; Itoh, H.; Podolsky, D. K. Distinct  
pathways of cell migration and antiapoptotic response to epithelial  
injury: structure-function analysis of human intestinal trefoil factor.  
*Mol. Cell. Biol.* **2000**, *20*, 4680–4690.
- (73) Sun, Z. R.; Liu, H. M.; Yang, Z. Z.; Shao, D. B.; Zhang, W.;  
Ren, Y.; Sun, B. D.; Lin, J. F.; Xu, M.; Nie, S. N. Intestinal trefoil  
factor activates the PI3K/Akt signaling pathway to protect gastric  
mucosal epithelium from damage. *Int. J. Oncol.* **2014**, *45*, 1123–1132.
- (74) Hanisch, C.; Sharbati, J.; Kutz-Lohroff, B.; Huber, O.;  
Einspanier, R.; Sharbati, S. TFF3-dependent resistance of human  
colorectal adenocarcinoma cells HT-29/B6 to apoptosis is mediated  
by miR-491-5p regulation of lncRNA PRINS. *Cell Death Discovery*  
**2017**, *3*, No. 16106.
- (75) Liu, J.; Kim, S. Y.; Shin, S.; Jung, S.-H.; Yim, S.-H.; Lee, J. Y.;  
Lee, S.-H.; Chung, Y.-J. Overexpression of TFF3 is involved in  
prostate carcinogenesis via blocking mitochondria-mediated apopto-  
sis. *Exp. Mol. Med.* **2018**, *50*, 1–11.
- (76) Wang, J.; Yadav, V.; Smart, A. L.; Tajiri, S.; Basit, A. W. Toward  
oral delivery of biopharmaceuticals: an assessment of the gastro-  
intestinal stability of 17 peptide drugs. *Mol. Pharmaceutics* **2015**, *12*,  
966–973.
- (77) Braga Emidio, N.; Tran, H. N. T.; Andersson, A.; Dawson, P.  
E.; Albericio, F.; Vetter, I.; Muttenthaler, M. Improving the  
gastrointestinal stability of linaclotide. *J. Med. Chem.* **2021**,  
DOI: 10.1021/acs.jmedchem.1c00380.
- (78) Hirel, P. H.; Schmitter, J. M.; Dessen, P.; Fayat, G.; Blanquet, S.  
Extent of N-terminal methionine excision from *Escherichia coli*  
proteins is governed by the side-chain length of the penultimate  
amino-acid. *Proc. Natl. Acad. Sci. U.S.A.* **1989**, *86*, 8247–8251.
- (79) Baumann, L.; Prokoph, S.; Gabriel, C.; Freudenberg, U.;  
Werner, C.; Beck-Sickinge, A. G. A novel, biased-like SDF-1  
derivative acts synergistically with starPEG-based heparin hydrogels  
and improves eEPC migration in vitro. *J. Controlled Release* **2012**, *162*,  
68–75.
- (80) Wanka, L.; Babilon, S.; Kaiser, A.; Mörl, K.; Beck-Sickinge, A.  
G. Different mode of arrestin-3 binding at the human Y1 and Y2  
receptor. *Cell. Signalling* **2018**, *50*, 58–71.